Next non-Gaussianity frontier: What can a measurement with $\sigma(f_{\rm NL}) \lesssim 1$ tell us about multifield inflation?

Roland de Putter,[1] Jérôme Gleyzes,[1,2] and Olivier Doré[1,2]

[1]*California Institute of Technology, MC 367-17, Pasadena, California 91125, USA*
[2]*Jet Propulsion Laboratory, California Institute of Technology,
4800 Oak Grove Drive, Pasadena, California 91109, USA*
(Received 2 January 2017; published 8 June 2017)

Future galaxy surveys promise to probe local primordial non-Gaussianity at unprecedented precision, $\sigma(f_{\rm NL}) \lesssim 1$. We study the implications for multifield inflation by considering spectator models, where inflation is driven by the inflaton field, but the primordial perturbations are (partially) generated by a second, spectator field. We perform a Markov chain Monte Carlo likelihood analysis using Planck data to study quantitative predictions for $f_{\rm NL}$ and other observables for a range of such spectator models. We show that models where the primordial perturbations are dominated by the spectator field, while fine-tuned within the broader parameter space, typically predict $f_{\rm NL}$ of order unity. Therefore, upcoming galaxy clustering measurements will constitute a stringent test of whether or not the generation of primordial perturbations and the accelerated expansion in the inflationary universe are due to separate phenomena.

I. INTRODUCTION

Inflation is the leading theory describing the early Universe [1–4], addressing both the standard problems of the hot big bang model (horizon problem, etc) and generating the primordial curvature fluctuations that are the seeds of the structure of the Universe observed today. All this can be achieved, in a manner consistent with all current data, with the introduction of a single scalar field. However, there is no theoretical reason to expect only one field to be important in the early Universe, and indeed fundamental physics models, such as those rooted in string theory, commonly predict multiple scalar fields (e.g. [5–7]). Moreover, multifield models provide an alternative important for falsifying the single-field paradigm.

A critical method for testing the single- vs. multifield nature of inflation is to look for local primordial non-Gaussianity (PNG), characterized by the parameter $f_{\rm NL}^{\rm loc}$ [8] (since we exclusively consider PNG of the local type, we will often omit the qualifier "local"). While single-field models predict negligible local PNG [9,10], $f_{\rm NL} = -5/12(n_s - 1)$ (see e.g. [11,12] for caveats to this rule), where n_s is the scalar spectral index, multifield models can generate observably large $f_{\rm NL}$ (see [13] for a review). The strongest current limits on $f_{\rm NL}$ come from the bispectra of cosmic microwave background (CMB) fluctuations, observed by the Planck satellite, $f_{\rm NL} = 0.8 \pm 5.0$ [14]. However, near-future galaxy surveys have the potential to improve on this significantly [15], taking advantage of an exciting new signal. In the presence of local PNG, the bias of galaxy density perturbations relative to the underlying matter density receives a scale-dependent correction, with scaling $\Delta b(k) \propto k^{-2}$ (where k is the wave number), which becomes important on scales comparable to the Hubble

scale [16–19]. By probing this characteristic signal on ultra-large scales, upcoming surveys such as SPHEREx [20–22], LSST [23] and EUCLID [24] are expected to improve on the current Planck constraint,[1] eventually leading to order unity precision [26–29], $\sigma(f_{\rm NL}) \lesssim 1$.

The motivation of this article is to address, in a quantitative way, what such a future $f_{\rm NL}$ constraint can teach us about multifield inflation, and what signal we might expect to find.

While in single-field models the curvature perturbations are conserved from the time the modes of interest exit the horizon, in multifield inflation the perturbations can undergo super-horizon evolution after this time. This leads to a rich and complex phenomenology, where the final non-Gaussianity may strongly depend on physics both during and after inflation, including the reheating process. While large $f_{\rm NL}$ is not generic in multifield inflation, often requiring significant fine-tuning [30], a number of interesting models have been identified where large (by *large* we mean $|f_{\rm NL}| \gtrsim 1$) non-Gaussianity is generated. Examples include the curvaton [31–35], modulated reheating [36–40], models with an inhomogeneous end to inflation [41–44], the axion-quadratic model where an adiabatic limit is reached before reheating [45–47], two-field models with non-Gaussianity generated during slow-roll inflation [30], hybrid inflation [48,49], N-flation [6,50,51], modulated trapping [52], and velocity modulation [53].

Although many previous studies have provided useful general, analytic insights into generation of non-Gaussianity in multifield inflation (see e.g. [30,54–56]), an alternative

---

[1]Next-generation CMB missions may also significantly improve the $f_{\rm NL}$ constraint relative to the Planck limit, see e.g. [25].

approach is to use MCMC techniques to numerically sample the full parameter space of a number of multifield models (cf. [57–61]), given constraints from Planck on $f_{\rm NL}$, n_s and the tensor-to-scalar ratio r (and implicitly on the scalar amplitude A_s). This is the approach we will take here, paying specific attention to the predictions for the distribution of $f_{\rm NL}$ compared to $\sigma(f_{\rm NL}) \lesssim 1$. To compute the evolution of perturbations, and $f_{\rm NL}$ in particular, we will use the δN formalism [62–65].

Instead of attempting to somehow sample the full space of multifield models, we restrict ourselves to an interesting subset, so-called "spectator models" (see also e.g. [47, 66–68]), that capture key phenomenology of generating large $f_{\rm NL}$. As a matter of definition, we assume there are two fields during inflation, described by a separable potential: the *inflaton* field, ϕ, which at horizon exit dominates both the curvature perturbation and the background energy density, and a *spectator* field, χ, which is subdominant at this time, but the perturbations of which (partially) determine the final curvature perturbation. These models are a natural extension beyond single-field inflation, with the inflaton still "driving" inflation. In particular, in the "spectator-dominated" regime, where the final curvature perturbations are *dominated* by the spectator contribution, these models simply separate the two main features of inflation: the inflaton drives the background expansion, while the spectator generates the primordial power spectrum. Our main interest will be in this latter regime, as it is here that large $f_{\rm NL}$ can be produced.

In addition to simplifying calculations and thus allowing for easier insights, requiring χ to be subdominant during inflation (or at least at horizon exit) plays an important role in generating large $f_{\rm NL}$. The reason is that, quite commonly, if both fields individually have flat potentials (small ratios of the first and second derivatives relative to the potential itself, in Planck units), then $f_{\rm NL}$ is typically suppressed. However, if the potential of χ is small compared to the total energy density, it is allowed to have a "non-flat" potential while still satisfying the slow-roll conditions (since the latter depend on the ratios of potential derivatives to the *total* energy density). As we will see, evading this flat potential restriction is what makes it easier to generate large non-Gaussianity with the spectator field.

Since we wish to sample a concrete parameter space and compare to current data, we will study three specific spectator models (these models are not necessarily spectator models, but we will restrict them to the parameter space where they are), covering a range of mechanisms for converting perturbations in the spectator field into curvature perturbations: (A) a quadratic-axion potential, with conversion while both fields are rolling, (B) the curvaton, with conversion after the inflaton has decayed into radiation, and (C) modulated reheating, with conversion at the time of reheating.

By choosing specific models, our approach sacrifices generality, but the benefit is that we will be able to derive concrete, quantitative predictions for the probability distribution of $f_{\rm NL}$ and other quantities. In particular, it is commonly claimed that various models naturally generate order unity $f_{\rm NL}$ [15,40,56,69,70], which we will back up here with a complete likelihood analysis.

We will consider the following specific questions:
  (i) Do spectator-dominated models (which are the ones interesting for $f_{\rm NL}$) require fine-tuning of parameters?
 (ii) What is the posterior probability of finding $|f_{\rm NL}| \gtrsim 1$ in spectator-dominated models?
(iii) How does $f_{\rm NL}$ relate to model parameters, and what would measuring $f_{\rm NL} \sim 1$ tell us about the parameter space?
 (iv) What is the complementarity between primordial non-Gaussianity and searches for primordial tensor modes?

The article is organized as follows. In Sec. II, we review general formalism describing inflation and the primordial curvature perturbations. In Sec. III, we introduce spectator models in general and in particular the three scenarios of interest. In Sec. IV, we discuss the observational constraints that we will compare the models with. In Sec. V, we describe the results of our likelihood analysis of the three models and in Sec. VI, we provide a final discussion and summarize our results.

II. GENERAL FORMALISM

In single-field inflation, the comoving curvature perturbation on uniform density hypersurfaces, ζ [71], is nonlinearly conserved after horizon exit [72,73]. Thus, the statistics of ζ remain frozen through the subsequent evolution of the inflationary Universe and the potentially complicated phase of reheating. In particular, according to the powerful single-field consistency condition [9,10], the level of local non-Gaussianity remains frozen at the negligible value $f_{\rm NL} = -5/12(n_s - 1)$.

The situation in multifield inflation is more complicated. The additional field(s) lead to entropy perturbations at the time of horizon exit, which can be transferred into the curvature perturbation through super-horizon evolution, thus modifying the primordial power spectrum and non-Gaussianity of ζ. Eventually, inflation ends and reheating takes place, giving rise to the radiation dominated, conventional hot big bang phase. We will assume that here the Universe reaches a state of thermal equilibrium without non-local conserved quantum numbers, which implies that after reheating, perturbations are adiabatic, and ζ is conserved [74–76] until horizon reentry at a much later time. Thus, the statistics of ζ just after reheating describe the standard adiabatic primordial fluctuations and feed into the calculation of observational phenomena in the late(r)

Universe, such as the cosmic microwave background anisotropies and cosmological large-scale structure.

In the models considered in this work, entropy-to-curvature conversion, and in particular the generation of non-Gaussianity in ζ, can take place both during inflation and/or during the period between the end of inflation and the time of reheating. By the latter we mean the time reheating/thermalization completes and the hot big bang phase with adiabatic perturbations is reached. In the following, we will give a brief overview of our treatment of evolution during both of these phases, and of how the perturbations are computed. We mostly follow standard methods and refer to the vast literature, e.g. the reviews [13,77], for more details.

A. Background evolution

We will assume inflation is described by two scalar fields with a sum-separable potential,

$$W(\phi,\chi) \equiv U(\phi) + V(\chi). \tag{1}$$

The slow-roll parameters are then defined as,

$$\epsilon^\phi \equiv \frac{m_{\mathrm{Pl}}^2}{2}\left(\frac{U_\phi}{W}\right)^2, \qquad \eta^\phi \equiv m_{\mathrm{Pl}}^2 \frac{U_{\phi\phi}}{W}$$

$$\epsilon^\chi \equiv \frac{m_{\mathrm{Pl}}^2}{2}\left(\frac{V_\chi}{W}\right)^2, \qquad \eta^\chi \equiv m_{\mathrm{Pl}}^2 \frac{V_{\chi\chi}}{W}, \tag{2}$$

where a field subscript defines a derivative w.r.t. the field and $m_{\mathrm{Pl}} = (8\pi G)^{-1/2}$ is the *reduced* Planck mass (the standard Planck mass is $M_{\mathrm{Pl}} = \sqrt{8\pi}m_{\mathrm{Pl}}$). We work in natural units, $c = \hbar = 1$. We also define a total slow-roll parameter $\epsilon \equiv \epsilon^\phi + \epsilon^\chi$, which to leading order in slow-roll parameters equals $\epsilon_H \equiv -\dot{H}/H^2$. Making the standard slow-roll assumption (i.e. taking the slow-roll parameters above to be small), the Friedmann equation takes the form,

$$3m_{\mathrm{Pl}}^2 H^2 = U(\phi) + V(\chi), \tag{3}$$

where $H = \dot{a}/a$ is the Hubble rate (dots denote time derivatives). Under the same slow-roll approximation, the equations of motion for the fields read,

$$3H\dot{\phi} = -U_\phi \qquad 3H\dot{\chi} = -V_\chi. \tag{4}$$

The above describes the background evolution during inflation while both fields are slowly rolling. After this period, but before reheating, there are many possible scenarios. We will discuss several of these in more detail in the upcoming sections about the three specific models of interest. Broadly speaking, there are two main types of transitions. For a field of mass m, when the Hubble rate

drops down to $H = m$, the field starts oscillating around the minimum of its potential. Assuming the potential is quadratic around this minimum, the energy density of the field, averaged over oscillation cycles, decays like that of pressureless matter, $\rho \propto a^{-3}$, where a is the cosmic scale factor.

The second type of transition takes place when a field converts its energy into radiation through decays or non-perturbative particle production. This reheating process is generally very complex, but we will model it in a simple way by assuming that reheating occurs instantaneously when $H = \Gamma$, where Γ is a decay rate to particles in the post-inflationary heat bath. The instantaneous reheating approximation is commonly made in the literature [34, 78–80], but it must be noted that a more realistic treatment of reheating could non-negligibly alter the predictions for the primordial perturbations (see [81] for a review). After this transition, the energy density formerly in the field decays like $\rho \sim a^{-4}$. We will consider scenarios where the two fields are converted to radiation at different times. When used without specific context, we will reserve the term "reheating" for the final process leading to the hot big bang phase.

B. Perturbations

We compute the evolution of perturbations by taking advantage of the separate Universe/δN formalism [62–65], which allows us to express the curvature perturbation in terms of field perturbations $\delta\phi_*$, $\delta\chi_*$ at the time of horizon exit, t_*. In the large-scale limit, $k \to 0$, we can treat perturbed regions of the Universe as separate FLRW universes obeying the background equations. The evolution of perturbations can then simply be obtained by considering the difference between background quantities in these separate universe patches. In particular, the curvature perturbation ζ can be computed in terms of the difference in the number of e-foldings of evolution between two patches. Specifically, at t_*, on a spatially flat hypersurface, consider a patch of the Universe at $\mathbf{x}$. Then, the curvature perturbation ζ at some later time t_c is simply the perturbation to the number of e-foldings of expansion needed to get from t_* to the constant energy density hypersurface, $\delta\rho = 0$, at time t_c. In terms of the initial field perturbations on a spatially flat hypersurface, $\delta\phi_* \equiv \phi(t_*,\mathbf{x}) - \phi(t_*)$, $\delta\chi_* \equiv \chi(t_*,\mathbf{x}) - \chi(t_*)$ (where $\phi(t_*)$ and χ_* are the background values),

$$\zeta(t_c) = \delta N(t_*, t_c)$$

$$= N_{\phi_*}\delta\phi_* + N_{\chi_*}\delta\chi_* + \frac{1}{2}N_{\phi_*\phi_*}\delta\phi_*^2$$

$$+ \frac{1}{2}N_{\chi_*\chi_*}\delta\chi_*^2 + N_{\phi_*\chi_*}\delta\phi_*\delta\chi_* + \cdots, \tag{5}$$

where we have dropped the position coordinate $\mathbf{x}$, and on the right hand side also the time dependence. Here,

$$N(t_*, t_c) = \int_*^c dt H(t),$$ (6)

and $N_{\phi_*} = \partial N / \partial \phi_*$, etc.

The δN formalism thus allows us to compute perturbations purely in terms of the evolution of slightly different FLRW background universes. Note that by writing ζ in terms of $\delta \phi_*$ and $\delta \chi_*$ only, we have implicitly assumed the perturbations have reached the space of inflationary growing/attractor solutions. In general, a model with two fields has four degrees of freedom, $\delta \dot{\phi}$ and $\delta \dot{\chi}$ in addition to $\delta \phi$ and $\delta \chi$ (defined on a hypersurface of zero spatial curvature). However, by assuming the slow-roll approximation, we have turned second order equations of motion into first order ones, thus reducing the effective number of degrees of freedom to two.

Note finally that at t_*, we have to first order,

$$\zeta_* = \frac{\sqrt{2\epsilon_*^\phi}}{2\epsilon_* m_{\rm Pl}} \delta\phi_* + \frac{\sqrt{2\epsilon_*^\chi}}{2\epsilon_* m_{\rm Pl}} \delta\chi_*,$$ (7)

and the non-Gaussianity in ζ_* is negligible [82]. The above expression in terms of the slow-roll parameters assumes that the potential slopes are positive. Negative slopes lead to corresponding minus signs in the above expression.

C. Connecting to observation

In the δN formalism, the dimensionless power spectrum of curvature perturbations is given by

$$\mathcal{P}_\zeta = \frac{k^3 P_\zeta}{2\pi^2} = \mathcal{P}_* (N_{\phi_*}^2 + N_{\chi_*}^2), \quad \text{with}$$

$$\mathcal{P}_* = \left(\frac{H_*}{2\pi}\right)^2,$$ (8)

where $\mathcal{P}_*$ is the dimensionless power spectrum of the field perturbations $\delta\phi_*$ and $\delta\chi_*$ at horizon exit, and H_* is the Hubble parameter at t_*. A useful quantity in the following is the fraction of the primordial power spectrum generated by the field χ,

$$R \equiv \frac{\mathcal{P}_\zeta|_\chi}{\mathcal{P}_\zeta} = \frac{N_{\chi_*}^2}{N_{\phi_*}^2 + N_{\chi_*}^2}.$$ (9)

In addition to the amplitude, another important observational property of the primordial power spectrum is the spectral index n_s. Taking the derivative of the power spectrum (8), one can express this quantity in terms of the slow-roll parameters at t_* [65,83],

$$n_s - 1 = -2\epsilon_* + 2R\eta_*^\chi + 2(1-R)\eta_*^\phi - \frac{2}{m_{\rm Pl}^2(N_{\phi_*}^2 + N_{\chi_*}^2)}$$ (10)

Similarly, the tensor-to-scalar ratio is given by,

$$r = \frac{8}{m_{\rm Pl}^2(N_{\phi_*}^2 + N_{\chi_*}^2)}.$$ (11)

Finally, the local non-Gaussianity parameter is,[2]

$$f_{\rm NL} = \frac{5}{6}\left[(1-R)^2 \frac{N_{\phi_*\phi_*}}{N_{\phi_*}^2} + R^2 \frac{N_{\chi_*\chi_*}}{N_{\chi_*}^2} \right.$$
$$\left. + 2R(1-R)\frac{N_{\phi_*\chi_*}}{N_{\phi_*}N_{\chi_*}}\right]$$ (12)

Thus, non-Gaussianity can be generated through nonlinear evolution of initial field perturbations into the curvature perturbation. The expression above neglects a small, slow-roll suppressed contribution due to intrinsic non-Gaussianity in $\delta\phi_*$ and $\delta\chi_*$ [82].

Finally, we note that in the presence of local non-Gaussianity, the statistics of ζ (the amplitude of the primordial power spectrum, $f_{\rm NL}$, etc.) observable in our local Hubble volume may differ from the global statistics [84–86] due to modes on scales larger than our Hubble volume giving rise to field perturbations with non-zero mean in our Hubble volume. Indeed, if we interpret the field values at horizon exit, ϕ_* and χ_*, as the *global* background values, the statistics predicted in the standard formalism discussed above only describe our Hubble volume if the mean perturbations in our Hubble volume to these fields are zero. However, we could also interpret ϕ_*, χ_* as the *local* background values in our Hubble volume (i.e. absorbing the super-Hubble volume perturbations), in which case the predictions of the standard formalism are directly applicable. This is not unreasonable as even the global initial field values are *a priori* unknown free parameters anyway.

III. SPECTATOR MODELS

As motivated in the Introduction, in this paper we focus on spectator models, which we will review in this section. We define these here by requiring that the initial curvature perturbation at horizon exit, ζ_*, is dominated by the perturbation in the inflaton ϕ. This requirement is satisfied if the slow-roll parameter ϵ_*^ϕ is much larger than ϵ_*^χ (cf. Eq. (7)). The perturbation $\delta\chi_*$ then describes an isocurvature/entropy perturbation. We also separately require that the energy density of the Universe at the time of horizon exit is dominated by the inflaton potential, i.e. at this time inflation is "driven" by the inflaton field. In equations, this comes down to,

---

[2]Note that we use a sign convention consistent with Planck, but opposite to that of [9,65].

$$\epsilon_*^\phi \gg \epsilon_*^\chi \quad \text{and} \quad U_* \gg V_* \quad \textbf{spectator models}$$

In these models, the parameter R now distinguishes between the regimes where the final curvature power spectrum is dominated by inflaton (ϕ) or spectator (χ) fluctuations,

$$R \approx 0 : \textbf{ Inflaton-dominated regime}$$

$$R \approx 1 : \textbf{ Spectator-dominated regime}$$

The spectator-dominated regime is particularly interesting for the generation of observable levels of non-Gaussianity and is the main focus of this work.

In the spectator limit, where in particular $\epsilon_*^\phi \gg \epsilon_*^\chi$, a pure (i.e. at fixed χ) initial inflaton fluctuation $\delta\phi_*$ describes an adiabatic perturbation,[3] which corresponds to a conserved curvature perturbation ζ. Therefore, in spectator models, we have

$$N_{\phi_*} \approx \frac{1}{\sqrt{2\epsilon_*}m_{\rm Pl}} \approx \text{const.}, \tag{13}$$

so that the final power spectrum is given by,

$$\mathcal{P}_\zeta \approx \frac{1}{1-R}P_{\zeta,*} = \frac{1}{1-R}\frac{1}{2\epsilon_*m_{\rm Pl}^2}\left(\frac{H_*}{2\pi}\right)^2. \tag{14}$$

Thus, the conversion of entropy to curvature can only increase the power spectrum, leading to a large boost in power in the spectator-dominated regime. The scalar spectral index, Eq. (10), for spectator models simplifies to,

$$n_s - 1 = -2\epsilon_* + 2R\eta_*^\chi + 2(1-R)(\eta_*^\phi - 2\epsilon_*), \tag{15}$$

so that it varies between

$$n_s - 1 = -6\epsilon_* + 2\eta_*^\phi \quad \text{(inflaton-dominated regime)}$$

$$n_s - 1 = -2\epsilon_* + 2\eta_*^\chi \quad \text{(spectator-dominated regime)}$$

Note that both asymptotic values are of order slow-roll, and are entirely determined by the slow-roll parameters at horizon exit.

Since the tensor power spectrum remains constant after horizon exit, the tensor-to-scalar ratio for spectator models is suppressed for $R > 0$,

---

[3]In general, one can define the initial adiabatic field perturbation as $(\delta\phi_*, \delta\chi_*)_{\rm ad} \equiv \delta\varphi_*(\sqrt{2\epsilon^\phi}/\sqrt{2\epsilon}, \sqrt{2\epsilon^\chi}/\sqrt{2\epsilon}) \propto (\dot{\phi}, \dot{\chi})$ (where we assumed the slopes of the potentials to have the same sign and we have used the slow-roll approximation). In other words, $\delta\varphi_*$ describes a perturbation along the background field trajectory. The normalization is chosen such that $\delta\varphi_*$ can be obtained by a local rotation in field space. One then has $N_{\varphi_*} = 1/\sqrt{2\epsilon_*}$ (cf. Eq. (7)), which is conserved.

$$r = 16(1-R)\epsilon_*. \tag{16}$$

The suppression of r in the spectator-dominated regime is both a feature and a bug. On the one hand, it becomes exceedingly difficult to detect primordial tensor modes observationally. On the other hand, large-field inflaton models that are currently ruled out because they predict a value of r above the observationally allowed range can be put in concordance with the data by adding a spectator field that seeds a large fraction of the primordial power spectrum (we will discuss this further in Sec. V D).

Regarding the non-Gaussianity in spectator models, the general expression for $f_{\rm NL}$ in Eq. (12) contains three terms. In the spectator limit, in particular when $\epsilon_*^\phi \gg \epsilon_*^\chi$ [cf. discussion above Eq. (13)], an initial perturbation in the inflaton direction ($\delta\chi_* = 0$) is to a good approximation an adiabatic perturbation. For such a perturbation, in the δN formalism, $\zeta = \delta N$ at any time is then approximately given simply by the contribution at the time of horizon exit from the perturbation $\delta\phi_*$ along the background trajectory (and is therefore approximately conserved), $N_\phi \approx U(\phi_*)/U_\phi(\phi_*)$, etc. This means that N_ϕ and $N_{\phi\phi}$ are given by the same expressions as in single-field inflation and in particular that $N_{\phi\phi}/N_\phi^2$ is slow-roll suppressed as in single-field inflation. Moreover, since in this limit, N_ϕ is a function of ϕ only, $N_{\phi\chi}$ is equal to zero. Thus, the $N_{\phi\phi}$ and $N_{\phi\chi}$ terms in Eq. (12) are negligible for our purposes (we remind the reader that we are focused on probing $f_{\rm NL}$ with order unity precision), allowing the following approximation,

$$f_{\rm NL} = \frac{5}{6}R^2\frac{N_{\chi_*\chi_*}}{N_{\chi_*}^2}. \tag{17}$$

We will see that the above expression can give rise to large $f_{\rm NL}$ for $R \sim 1$.

We will discuss this more quantitatively in Sec. V D, but we see here already the complementarity between measuring primordial tensor fluctuations and non-Gaussianity (of the scalar fluctuations). For large-field inflaton potentials in the inflaton-dominated regime, r is within reach of empirical tests, but $f_{\rm NL}$ is too small to be detected in the near future, whereas in the spectator-dominated regime, r is strongly suppressed and difficult to detect, but $f_{\rm NL}$ can be within observational reach.

A. Three specific spectator models

In the following sections, we will introduce the three specific spectator models for which we will study observational predictions and constraints. For the spectator field potential, $V(\chi)$, we will consider both an axion-like periodic potential and a quadratic potential, which we will discuss in more detail further below.

For the inflaton field, we consider simple, large-field (e.g. power law) potentials. Since our main interest is in the properties of the spectator field and how it generates f_{NL}, the details of $U(\phi)$ are less important for our study than the properties of χ and the transfer of its perturbations. The spirit of our approach to the inflaton potential is that there is in principle ample freedom in its form to always be able to fit at least n_s and A_s, and that f_{NL} is relatively insensitive to the details of $U(\phi)$. In practice, to keep the calculations as simple as possible, our main implementation of the inflaton potential will be a quadratic potential,

$$U(\phi) = \frac{1}{2} m_\phi^2 \phi^2, \qquad (18)$$

where we treat the field value at horizon exit, ϕ_*, as a free parameter. We will briefly consider a more general setup, with varying power law index of the inflaton potential, in Sec. V D.

1. Case A: The quadratic-axion in the horizon crossing approximation

We first consider a model where the spectator field is governed by a periodic, axionlike potential,

$$V(\chi) = \frac{1}{2} V_0 \left[1 + \cos\left(\frac{2\pi\chi}{f} \right) \right], \qquad (19)$$

where f is a "decay constant", and V_0 gives the normalization of the potential. In the case under consideration, where the inflaton is described by a quadratic potential, this is the quadratic-axion model [45–47]. This is a known, simple example of a model capable of generating large non-Gaussianity ($|f_{NL}| \gtrsim 1$) during or slightly after slow-roll inflation without necessarily relying on mechanisms during the reheating phase. We explain below why this is, after introducing the approximation we will use to compute perturbations in this model. The assumption of a quadratic potential for the inflaton is not crucial so that the quadratic-axion model is merely a specific example of a broader class of "inflaton-axion" models.

During inflation, while both fields obey the slow-roll conditions, the number of e-foldings between t_* and some later time t_c, is given by[4]

$$N = -\frac{1}{m_{Pl}^2} \int_{\phi_*}^{\phi_c} \frac{U}{U_\phi} d\phi - \frac{1}{m_{Pl}^2} \int_{\chi_*}^{\chi_c} \frac{V}{V_\chi} d\chi. \qquad (20)$$

---

[4]The case of a sum-separable potential during slow-roll is special in the sense that N can be written as a path-independent integral through field space. In other words, there exists some function defined for all ϕ and χ, and N is simply the difference of that function between the end point (ϕ_c, χ_c) and the starting point (ϕ_*, χ_*). It is this property that allows the derivation of closed analytic expressions for the curvature perturbation as in [65].

Assuming a zero spatial curvature hypersurface at t_* and a constant energy density surface at t_c, the δN formalism allows us to write the curvature perturbation at t_c as

$$\zeta(t_c) = \delta N = \left[\frac{1}{m_{Pl}^2} \left(\frac{U}{U_\phi} \right)_* \delta\phi_* + \frac{1}{m_{Pl}^2} \left(\frac{V}{V_\chi} \right)_* \delta\chi_* \right]$$
$$- \left[\frac{1}{m_{Pl}^2} \left(\frac{U}{U_\phi} \right)_c \delta\phi_c + \frac{1}{m_{Pl}^2} \left(\frac{V}{V_\chi} \right)_c \delta\chi_c \right], \qquad (21)$$

which is straightforwardly extended to higher orders. Since we have fixed the gauge at t_c, the perturbations $\delta\phi_c$ and $\delta\chi_c$ are fully specified in terms of $\delta\phi_*$ and $\delta\chi_*$. This enabled [65] to derive analytic expressions for ζ in terms of $\delta\phi_*$ and $\delta\chi_*$ only. The $\delta\phi_c$ and $\delta\chi_c$ contributions make these expressions rather complicated.

The horizon crossing approximation (HCA). If, however, before t_c, an adiabatic limit is reached where, independently of the initial perturbation, the fields always end up on the same field trajectory, the contributions from the perturbations at t_c can be neglected. In this limit, the perturbations are well described by the so-called horizon crossing approximation (HCA) [45,50,87] and are fully expressed in terms of the field perturbations at horizon exit (we note that, in single-field inflation, this assumption is generally satisfied at all times after horizon exit under the standard assumption of being on the single-field attractor solution, thus explaining why ζ is conserved in single-field inflation). The HCA simplifies the expressions for the perturbations and their non-Gaussianity considerably, giving easy insights in the multifield phenomenology and allowing us to straightforwardly identify models with the potential for generating large non-Gaussianity.

Before explicitly writing the HCA expressions to second order, it is useful to define slow-roll parameters for the individual potentials [cf. Eq. (2)],

$$\tilde{\epsilon}^\phi \equiv \frac{m_{Pl}^2}{2} \left(\frac{U_\phi}{U} \right)^2, \qquad \tilde{\eta}^\phi \equiv m_{Pl}^2 \frac{U_{\phi\phi}}{U}$$

$$\tilde{\epsilon}^\chi \equiv \frac{m_{Pl}^2}{2} \left(\frac{V_\chi}{V} \right)^2, \qquad \tilde{\eta}^\chi \equiv m_{Pl}^2 \frac{V_{\chi\chi}}{V}. \qquad (22)$$

While the true slow-roll parameters, normalized by the total energy density W, are required to be small for the slow-roll approximations to hold, the individual slow-roll parameters can in principle be larger than unity. In particular, for spectator models, $\tilde{\epsilon}_*^\phi \approx \epsilon_*^\phi \approx \epsilon_*$, $\tilde{\eta}_*^\phi \approx \eta_*^\phi$, but $\tilde{\epsilon}_*^\chi = (W_*/V_*)^2 \epsilon_*^\chi \gg \epsilon_*^\chi$, $\tilde{\eta}_*^\chi = (W_*/V_*)\eta_*^\chi \gg \eta_*^\chi$.

In terms of these, the HCA gives

$$m_{\rm Pl} N_{\phi_*} = \frac{1}{\sqrt{2\tilde{\epsilon}_*^\phi}}, \qquad m_{\rm Pl} N_{\chi_*} = \frac{1}{\sqrt{2\tilde{\epsilon}_*^\chi}}$$

$$m_{\rm Pl}^2 N_{\phi_*\phi_*} = 1 - \frac{\tilde{\eta}_*^\phi}{2\tilde{\epsilon}_*^\phi}, \qquad m_{\rm Pl}^2 N_{\chi_*\chi_*} = 1 - \frac{\tilde{\eta}_*^\chi}{2\tilde{\epsilon}_*^\chi}, \qquad (23)$$

and $N_{\phi_*\chi_*} = 0$. Thus, assuming a spectator model, to be in the spectator-dominated regime, say $N_{\chi_*}^2 > N_{\phi_*}^2$, one requires

$$\tilde{\epsilon}_*^\chi < \tilde{\epsilon}_*^\phi \simeq \epsilon_*. \qquad (24)$$

This means one needs a very small value of $\tilde{\epsilon}_*^\chi$. Next, assuming the spectator domination requirement is fully satisfied ($R \approx 1$), the non-Gaussianity is given by

$$f_{\rm NL} \sim \frac{5}{6} \frac{N_{\chi_*\chi_*}}{N_{\chi_*}^2} = \frac{5}{6}(2\tilde{\epsilon}_*^\chi - \tilde{\eta}_*^\chi) \approx -\frac{5}{6}\tilde{\eta}_*^\chi. \qquad (25)$$

Therefore, for a spectator dominated model to generate large non-Gaussianity, one needs a large individual slow-roll parameter $|\tilde{\eta}_*^\chi| \gtrsim 1$. This is not inconsistent with slow-roll inflation because η_*^χ is suppressed relative to $\tilde{\eta}_*^\chi$. This argument (based on the simple HCA assumption), nicely illustrates the more general point that, in multifield inflation, if both fields contribute significantly to the energy density of the Universe, the slow-roll conditions typically restrict $f_{\rm NL}$ to be small, and that this limitation can be evaded by considering spectator fields, which may have very non-flat potentials without violating slow-roll because their energy density contribution is small.

The requirements of ultra-small $\tilde{\epsilon}^\chi$ and large $\tilde{\eta}^\chi$ are naturally incorporated in the axion model, Eq. (19), if the initial field χ_* is placed near the top of the cosine potential. In the limit $\chi_*/f \to 0$, the slope of the potential asymptotes to zero, while the curvature approaches a constant, thus satisfying the two conditions. By having the amplitude V_0 low, the slow-roll conditions are satisfied as well. This ability to produce large $f_{\rm NL}$, together with the fact that axion potentials can be realized in a technically natural way from a more complete Lagrangian, makes the inflaton-axion model theoretically appealing.

To illustrate the background evolution of the fields in this model, we schematically plot the energy densities as a function of the number of e-folds N in Fig. 1. We show two scenarios. In both, the energy density of χ is subdominant throughout the inflationary period driven by the inflaton ϕ. In the first scenario, χ starts rolling with its energy density decaying according to $\rho_\chi \propto a^{-3}$ slightly before the end of inflation (dark blue curve). After this, inflation ends, and both components decay like matter. Later, reheating takes place, after which we assume the total energy density of the Universe to exist in the form of radiation (thick red curve).
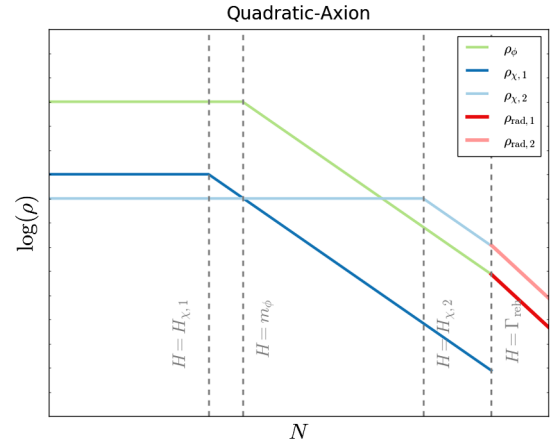

Quadratic-Axion

FIG. 1.   Illustration of the behavior of the background densities in the quadratic-axion scenario (case A), as a function of the number of e-folds N. We show two scenarios, depending on whether the spectator field/axion, χ, starts rolling down its potential before (dark blue) or after (light blue) the end of inflation. As illustrated, in the latter case, χ could generate a brief second phase of inflation before it starts oscillating. We assume that reheating only occurs after the phase is reached where both energy densities decay like $\rho \sim a^{-3}$ and that the reheating process does not alter the curvature perturbations. After reheating, the Universe is filled with radiation (thick red and pink for scenario 1 and 2 respectively) with adiabatic perturbations.

In the alternative scenario, χ starts rolling/oscillating after the end of inflation. While not always the case, in the scenario shown, this happens *after* χ has come to dominate the energy budget of the Universe, thus leading to a second phase of inflation of modest duration. Again, after both fields end up decaying proportional to a^{-3}, reheating takes place, and the Universe is filled with radiation (thick pink).

Which scenario takes place depends on the model parameters in a relatively straightforward manner. The time that χ starts rolling (exits slow-roll) is partially determined by comparing the Hubble rate to the mass associated with the axion potential,

$$m_\chi^2 \equiv \frac{2\pi^2}{f^2} V_0. \qquad (26)$$

Tuning the initial field value to be close to the hilltop, $\chi_*/f \ll 1$, however, will delay this moment. For $m_\chi > m_\phi$ and χ_*/f not too small, χ can thus start rolling before the end of inflation, as shown in scenario 1. If V_0 is sufficiently large, χ can also come to dominate the Universe before the end of inflation, thus lengthening the duration of inflation (not shown). In most cases relevant to our likelihood analysis, χ starts oscillating well after the end of inflation. For large f and small χ_*/f, χ first drives a second phase of inflation (scenario 2), but in a large fraction of parameter space, this is not the case, i.e. χ starts oscillating when its

energy density is smaller than or comparable to ρ_ϕ (not shown).

Validity of horizon crossing approximation. We now come back to the question of the range of validity of the HCA. The approximation is exact if an adiabatic limit is reached while both fields are in the slow-roll regime.[5] In practice, even if this is not the case, if after inflation a phase is reached where both fields oscillate around their minima (with energy densities decaying like $\rho \propto a^{-3}$), so that $\zeta = \text{const}$,[6] then the HCA still turns out to be a reasonable approximation in many cases (see e.g. [45]).

To test the range of validity of the HCA in the quadratic-axion model, we have numerically computed the perturbations into the $\zeta = \text{const}$ phase using the exact δN formalism and compared the results to the HCA predictions. We describe the details in Appendix B, but the main result is that, for the parameter space we will study here, the horizon crossing approximation is a good estimator of $f_{\rm NL}$ to within a factor of less than two. In addition, we introduce an f-dependent correction factor that brings the HCA prediction in much better agreement with the exact numerical calculation. We use both prescriptions separately in our likelihood analysis to bracket the possible range of $f_{\rm NL}$ values. Both prescriptions give qualitatively similar results.

Finally, for case A, we assume that reheating does not modify ζ after the $\zeta = \text{const}$ phase described by the HCA. In the simplified instantaneous reheating picture, this would correspond to reheating taking place on a constant total energy density hypersurface.

2. Case B: The curvaton

For case B, we consider a simple quadratic potential for the spectator field,

$$V(\chi) = \frac{1}{2} m_\chi^2 \chi^2. \qquad (27)$$

The curvaton scenario [31–35] relies on a post-inflationary phase where ϕ has already decayed into radiation and χ is oscillating around its minimum. Thus, the energy density of χ grows relative to that of ϕ and perturbations $\delta\chi$ are converted into curvature perturbations. It is known that in the limit where the curvature perturbations are dominated by $\delta\chi$, large non-Gaussianity ($|f_{\rm NL}| \gtrsim 1$) can be generated [78].

---

[5]When this is not the case, it is possible to modify ζ at the end of inflation through the dependence on $\delta\phi_c$ and $\delta\chi_c$ which is neglected in the HCA. In particular, models where the fields are on a turning trajectory at the end of inflation can generate large $f_{\rm NL}$ in a way not captured by the HCA.

[6]While ζ is constant in such a phase, this is not necessarily an adiabatic limit, as entropy perturbations may still exist. Only if these entropy perturbations are not converted to curvature through reheating at a later stage, will ζ remain constant into the hot big bang phase.
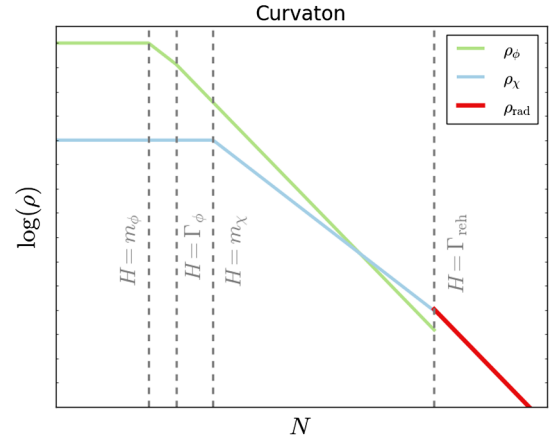

FIG. 2. Illustration of the behavior of the background densities in the curvaton scenario (case B). After the inflaton has decayed into radiation (at $H = \Gamma_\phi$), $\rho_\phi \sim a^{-4}$, an until then subdominant spectator/curvaton field χ starts oscillating around its potential minimum. Since $\rho_\chi \sim a^{-3}$ in this phase, its energy density may become important and its perturbations can be converted into curvature perturbations. This curvaton phase ends at $H = \Gamma_{\rm reh}$, when we assume χ decays into radiation with adiabatic fluctuations without further modifying the curvature perturbations.

Here, we consider the following specific curvaton scenario, with three main phases, as illustrated in Fig. 2. The first phase is the period of inflation, where both fields are slowly rolling. This phase ends when $H_{\rm end} = m_\phi$, at $t_{\rm end}$, after which the inflaton starts oscillating around its minimum, with energy density decaying like pressureless dust, $\rho_\phi \propto a^{-3}$. We assume that at some point during this phase, the inflaton decays into radiation, leading to $\rho_\phi \propto a^{-4}$ evolution (we keep using the subscript ϕ even though at this point the component consists of radiation). The second phase ends at $H_{\rm curv} = m_\chi < m_\phi$, at $t_{\rm curv}$, when the spectator field starts oscillating around its minimum, leading to $\rho_\chi = \frac{1}{2} m_\chi^2 \chi_{\rm curv}^2 (a/a_{\rm curv})^{-3}$. We refer to this third phase as the curvaton phase. It ends when also the curvaton decays into radiation at $H_{\rm reh} = \Gamma_{\rm reh} < m_\chi$. We assume all transitions take place on constant total energy density slices so that ζ is conserved across the transitions. While we assume throughout this paper that after reheating the perturbations are purely adiabatic, we refer to [59] for a recent study of the observational consequences of persisting isocurvature fluctuations.

For the curvaton scenario, we will make a slightly stronger assumption than the usual spectator requirements, namely that χ is subdominant not just at t_*, but until the beginning of the curvaton phase, $t_{\rm curv}$, i.e. $\frac{1}{2} m_\chi^2 \chi_{\rm curv}^2 \ll 3 m_{\rm Pl}^2 m_\chi^2$. This allows for simple analytic expressions for the spectator contributions to the final curvature perturbations [78] and for the evolution from χ_* to $\chi_{\rm curv}$. At the linear level, we use

$$N_{\chi_*} = \frac{2r_{\chi,\text{reh}}}{3\chi_*}, \qquad (28)$$

where χ_* is the initial field value and

$$r_\chi \equiv \frac{3\rho_\chi}{3\rho_\chi + 4\rho_\phi} \qquad (29)$$

gives the relative contribution of the curvaton to $\rho + p$ during the curvaton phase ($r_{\chi,\text{reh}} = r_\chi$ evaluated at t_{reh}). The non-Gaussianity parameter is given by

$$f_{\text{NL}} = \frac{5}{6}R^2\left(-r_{\chi,\text{reh}} - 2 + \frac{3}{2r_{\chi,\text{reh}}}\right). \qquad (30)$$

From Eq. (28), one needs small χ_* ($\lesssim \sqrt{2\epsilon_*}m_{\text{Pl}}$) to reach the spectator-dominated regime. Assuming $R \sim 1$ is indeed obtained during the curvaton phase, if this happens while r_χ is small, the non-Gaussianity can be very large $f_{\text{NL}} \sim 5/(4r_\chi)$. If and when the curvaton phase continues to the point where ρ_χ dominates ($r_\chi \to 1$), the asymptotic value $f_{\text{NL}} = -5/4$ is reached.

The results only minimally depend on exactly when during the second phase the inflaton decays into radiation.[7] Therefore, to keep the analysis minimal, instead of including a free parameter Γ_ϕ to describe this transition, we simply consider the extreme case, where ϕ decays immediately at t_{end}. We have checked that using the opposite extreme, where it decays at t_{curv}, leads to very similar results.

3. Case C: Modulated reheating

For case C, we again consider a simple quadratic potential for the spectator field,

$$V(\chi) = \frac{1}{2}m_\chi^2\chi^2. \qquad (31)$$

In the modulated reheating scenario [36–40] (see, e.g. [88,89] for recent studies), the decay rate of the inflaton, which determines the time of reheating, depends on the spectator field χ. Then, even if χ contributes negligibly to the energy density of the Universe, the quantum fluctuations in χ at horizon exit can be transferred into curvature perturbations through the reheating process (the reheating hypersurface is not one of constant energy density, but is modulated by χ). This is a well-known scenario producing large f_{NL} [40].

The specific case we consider here, see Fig. 3, consists of two phases: the standard inflationary phase, ending at $H_{\text{end}} = m_\phi$, and a subsequent phase where the inflaton

---

[7]Varying the time of decay slightly changes the evolution of χ between t_{end} and t_{curv} and therefore affects the curvaton energy density at t_{curv} and thus r_χ.
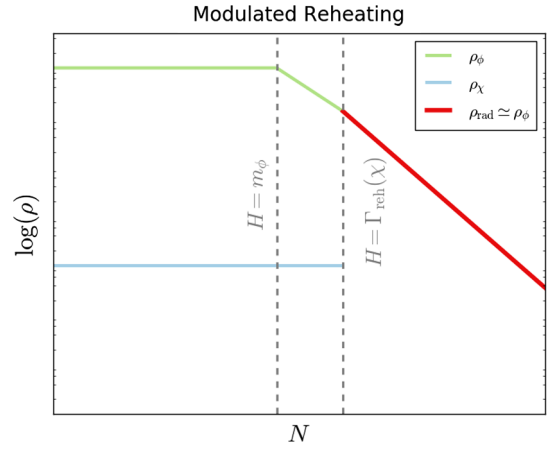

FIG. 3. Illustration of the behavior of the background densities in the modulated reheating scenario (case C). After inflation, the inflaton oscillates around its potential minimum and decays into radiation when $H = \Gamma_{\text{reh}}(\chi)$. The spectator field χ, which has negligible energy density at the time of reheating, modulates the hypersurface of reheating and may thus convert its fluctuations into curvature perturbations. We assume that after reheating by ϕ, the spectator field χ plays no further role (e.g. promptly decaying itself), leading to a Universe composed of radiation with adiabatic perturbations.

oscillates around its minimum and χ is still slowly rolling. This phase ends at t_{reh}, when $H_{\text{reh}} = \Gamma_{\text{reh}}(\chi)$. We assume χ is subdominant all the way up to t_{reh}, $\frac{1}{2}m_\chi^2\chi_{\text{reh}}^2 \ll 3\Gamma_{\text{reh}}^2(\chi_{\text{reh}})$, and that it plays no role in the generation of curvature perturbations other than through the reheating process. In particular, we assume that after t_{reh}, χ decays into radiation as well without further modifying ζ.

For the reheating of the inflaton, we consider a toy model where decay to fermions (q) is the dominant process, through a coupling term of the form,

$$\mathcal{L} \supset -\lambda(\chi)\phi\bar{q}q. \qquad (32)$$

The decay rate is then [90]

$$\Gamma_{\text{reh}} = \frac{m_\phi\lambda^2(\chi)}{8\pi}. \qquad (33)$$

For the dependence of the coupling constant on χ, we choose a simple expansion truncated at quadratic order (see also, e.g., [91,92]),

$$\lambda(\chi) = \lambda_0 + \lambda_1\frac{\chi}{M_c} + \frac{1}{2}\lambda_2\left(\frac{\chi}{M_c}\right)^2, \qquad (34)$$

where M_c is a cutoff scale in the effective field theory, $M_c \gg H_*$, and the dimensionless parameters $\lambda_0, \lambda_1, \lambda_2$ are at most of order unity (additional bounds are described in Appendix A).

Following [88], we use

$$N_{\chi_*} = -\frac{1}{6}\frac{\Gamma'_{\rm reh}}{\Gamma_{\rm reh}}\frac{\partial \chi_{\rm reh}}{\partial \chi_*}, \tag{35}$$

and

$$f_{\rm NL} = 5\left[1 - \frac{\Gamma_{\rm reh}\Gamma''_{\rm reh}}{(\Gamma'_{\rm reh})^2} - \frac{\Gamma_{\rm reh}}{\Gamma'_{\rm reh}}\left(\frac{\partial \chi_{\rm reh}}{\partial \chi_*}\right)^{-2}\frac{\partial^2 \chi_{\rm reh}}{\partial \chi_*^2}\right], \tag{36}$$

where primes denote derivatives w.r.t. $\chi_{\rm reh}$. We include the contributions due to the evolution of the spectator field between t_* and $t_{\rm reh}$ as in [88]. The expression for $f_{\rm NL}$ shows that, if the spectator-dominated regime is reached, one would naturally expect $|f_{\rm NL}| \sim 5$. We will make this more quantitative in Sec. V C.

IV. COMPARISON TO OBSERVATION

A. Current CMB constraints

We derive constraints on the three spectator models discussed above using the most recent Planck cosmic microwave background measurements [93] of n_s and $f_{\rm NL}$. For r, we use the joint analysis by Planck and BICEP2 of B-modes on the subset of the sky covered by BICEP2 [94] (which is why we will not include a correlation between n_s and r in our likelihood). Specifically, we model the measurements by Gaussian likelihoods (restricted to $r \geq 0$ for r) with mean and standard deviation,

$$n_s = 0.9645 \pm 0.0049, \tag{37}$$

$$r = 0.0497 \pm 0.0383, \tag{38}$$

where n_s and r are defined relative to a pivot scale $k_* = 0.05~{\rm Mpc}^{-1}$, and

$$f_{\rm NL} = 0.8 \pm 5.0. \tag{39}$$

We then apply standard Markov chain Monte Carlo (MCMC) techniques using the python package emcee [95] to derive constraints on the spectator parameters.

We summarize the parameter space and physically motivated priors for each model in Appendix A.

Planck also provides a measurement of the amplitude of the primordial power spectrum, $A_s \equiv \mathcal{P}_\zeta(k_*)$, namely [93,96]

$$\ln(10^{10}A_s) = 3.094 \pm 0.034. \tag{40}$$

We treat this measurement differently than the constraints on n_s, r and $f_{\rm NL}$. The reason is that we still have the freedom to take out an absolute energy scale from the equations describing our models by rescaling various

model parameters. We can choose this energy scale to be the normalization of the inflaton potential, in this case m_ϕ^2. Specifically, if we define rescaled quantities, $V(\chi) \to \tilde{V}(\chi) \equiv V(\chi)/m_\phi^2$, $m \to \tilde{m} \equiv m/m_\phi$, $\Gamma \to \tilde{\Gamma} \equiv \Gamma/m_\phi$, etc. (but leave the fields unchanged), the evolution equations retain the same form given previously, but in terms of the "tilded" quantities. The observables n_s, r and $f_{\rm NL}$ are also independent of the overall mass scale m_ϕ. The main quantity that does depends on m_ϕ is A_s. Therefore, we will in practice sample the rescaled parameters and, instead of also treating m_ϕ as a free parameter, it is implicit that at each point in parameter space it is tuned in order to obey the A_s constraint. One subtlety in this approach is that physical constraints and priors (see Appendix A) sometimes are naturally given in terms of absolute, not rescaled, scales. In order to translate these priors to the rescaled parameters, we will simply use a fiducial value for the overall mass scale, $m_\phi^{\rm fid} = 1.6 \times 10^{13}$ GeV (the mass scale required to reproduce the observed A_s for an inflaton-dominated model with $\phi_* = 15 m_{\rm Pl}$). This is a reasonable choice because the variation in m_ϕ needed to fit A_s is relatively small compared to the very wide prior ranges considered here.

In principle, there is a constraint in addition to the measurements of n_s, r, $f_{\rm NL}$ and A_s, namely on the number of e-foldings of inflation between horizon exit of the mode of interest and the end of inflation, N_*. Working backwards in time from the present, one can compute how far outside the horizon a given mode with wave vector k_* was at the time when inflation ends, which in turn specifies how many e-folds before the end of inflation that mode must have exited the horizon (see e.g. [93,97]),

$$N_* + \ln\left(\frac{H_{\rm end}}{H_*}\right) = 61.7 - \ln\left(\frac{k_*}{0.05~{\rm Mpc}^{-1}}\right)$$
$$- \frac{1}{12}\ln\left(\frac{g_*(T_{\rm reh})}{106.75}\right) + \frac{1}{4}\ln\left(\frac{H_{\rm end}^2}{3m_{\rm Pl}^2}\right)$$
$$+ \frac{1-3w_{\rm reh}}{12(1+w_{\rm reh})}\ln\left(\frac{H_{\rm reh}^2}{H_{\rm end}^2}\right). \tag{41}$$

Here, $w_{\rm reh}$ is the effective equation of state between the end of inflation and the finalization of the reheating phase, and $g_*(T_{\rm reh})$ is the effective number of degrees of freedom at the temperature of reheating.

Therefore, in those models considered here that specify the reheating history (cases B and C), the expansion history after the end of inflation fixes the number of e-foldings N_* before the end of inflation at which our mode of interest (at the pivot scale k_*) must have exited the horizon (technically, it fixes $N_* + \ln(H_{\rm end}/H_*)$). Thus, in these cases, the matching relation (41) in principle provides an additional constraint equation that essentially fixes ϕ_* in terms of the other parameters so that ϕ_* is not truly a free parameter. However, in principle, one could readily use the remaining

freedom to tune the shape of the inflaton potential (beyond the quadratic form) to match N_*. More specifically, for given values of ϕ_* and of the value of $N_* + \ln(H_{\mathrm{end}}/H_*)$ required by the postinflationary history, if we introduce additional parameters to describe an inflaton potential of more general form than the quadratic one (for instance promoting the power law index to a free parameter, or even going beyond the power law shape), we can in principle adjust the additional parameter(s) to satisfy the matching equation, thus leaving ϕ_* a free parameter. To keep our treatment as straightforward as possible, instead of adding new parameters describing a more general inflaton potential *and* applying the mode matching to N_*, we simply do neither and treat ϕ_* as a free parameter. Since, again, our main focus is the properties of the spectator field and f_{NL}, this minimally affects our results. In particular, f_{NL} is rather insensitive to these choices. We will briefly consider a more general setup, with varying power law index of the inflaton potential, in Sec. V D.

B. Future galaxy clustering constraints

Our MCMC runs exclusively include current CMB constraints. However, the motivation of this paper is to quantify the constraining power of next-generation measurements in the resulting space of multifield/spectator models allowed by current data. In particular, we are motivated by upcoming galaxy surveys, which, using scale-dependent halo bias, target order unity precision on local primordial non-Gaussianity, $\sigma(f_{\mathrm{NL}}) \lesssim 1$. Instead of modeling any specific survey, we will simply compare the posterior parameter and observable distributions from Planck data to this approximate level of constraint, $\Delta f_{\mathrm{NL}} \sim 1$.

V. RESULTS

A. The quadratic-axion in the horizon crossing approximation

We first consider the quadratic-axion model using the (improved) horizon crossing approximation; see Sec. III A 1 and Appendix B. The predictions of f_{NL} for this model will turn out to be very sensitive to the upper bound chosen for the "axion decay constant" f. Since in a UV complete theory, it may be difficult to generate axionlike potentials with f larger than the Planck scale [98,99], our default choice will be $f < M_{\mathrm{pl}} = \sqrt{8\pi}m_{\mathrm{Pl}}$ (note that M_{pl} is not the reduced Planck mass here). To illustrate the dependence on this cutoff, we will also show results for the prior $f < 3M_{\mathrm{pl}}$ (see Appendix A 1 for the other parameter priors).

In order to gain insight on what the allowed parameter space looks like, let us highlight what imposing the spectator-dominated regime means. Within the HCA, R has a very simple form and $R > 0.9$ translates into
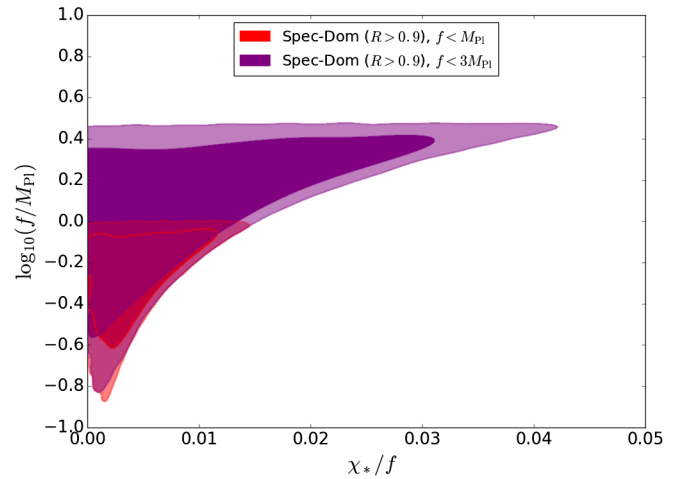

FIG. 4. The parameter region where the spectator field dominates the curvature perturbations ($R > 0.9$) in the quadratic-axion/HCA model (case A). Unless otherwise stated, we show 68% and 95% C.L. contours. We show results for two choices of prior, namely an upper bound on the "axion decay constant" $f < M_{\mathrm{Pl}}$ in red, and in purple a bound $f < 3M_{\mathrm{Pl}}$. The requirement $\chi_*/f \ll f$, cf. Eq. (42) and discussion in main text, is apparent.

$$\frac{\chi_*}{f} < \frac{f}{3\pi^2\phi_*}. \tag{42}$$

This behavior is clearly visible (specifically the contour edges at bottom-right) from Fig. 4, where we plotted the 2D 68% and 95% confidence level (C.L.) contours from our MCMC chains in the plane $(\chi_*/f, f)$, in the spectator-dominated (Spec-Dom) regime. Note that because of the form of the expressions in Eq. (23), R is independent[8] of V_0. The upper bounds in the vertical direction in Fig. 4 come directly from the priors on f. Throughout this paper, since bounds in the posterior parameter space are partially determined by (broad) priors, not just by the Planck measurements, the shapes of the posterior distributions commonly deviate from the narrow, Gaussian distributions one may find in a completely data dominated case with small error bars.

Since we envision χ/f as an axion *phase*, our prior expectation is for χ_* to be uniformly distributed in the interval $[0, f/2]$. Therefore, the requirement of very small χ_*/f in Eq. (42) corresponds to significant fine-tuning of initial conditions. Indeed, if we do not explicitly impose $R > 0.9$ in our MCMC runs, this condition is satisfied less than 1% of the time, while most of the points in the chains are concentrated in the inflaton-dominated $R \ll 1$ region, with $f_{\mathrm{NL}} \approx 0$. However, this region corresponds precisely to the case that is very similar to single-field inflation. In order to explore the features that are specific to the presence of the extra field, we will now focus on the

---

[8]In the HCA, the only place where V_0 explicitly appears is in the spectral index n_s, see Eq. (15).

spectator-dominated regime ($R > 0.9$), keeping in mind that this is a fine-tuned subset of models. In this regime, we are pushed towards large values of f, close to the prior upper bound, because large f allows for a larger range of initial field values satisfying Eq. (42).

The phenomenology of the background energy densities in the spectator-dominated parameter regime of $f \lesssim M_{\text{pl}}$, $\chi_*/f \lesssim f/(3\pi^2\phi_*)$ depends on the value of V_0/m_ϕ^2. For the largest values of this quantity allowed by the spectator requirement and by the constraint on η_*^χ coming from n_s, ρ_χ starts decaying like a^{-3} slightly before the end of inflation. However, given our broad prior, most of the posterior volume corresponds to much smaller values of V_0/m_ϕ^2. In that regime, χ starts oscillating well after inflation, when ϕ is already oscillating itself and ρ_ϕ decays like matter. In particular, for $f = M_{\text{pl}}$ and $\chi_*/f = f/(3\pi^2\phi_*)$, χ comes to dominate the total energy density of the Universe before it starts oscillating, leading to a short second phase of inflation (the second scenario in Fig. 1). Lowering f (still with $\chi_*/f = f/(3\pi^2\phi_*)$ and still assuming the low V_0/m_ϕ^2 regime), the ratio ρ_χ/ρ_ϕ at the time when χ starts oscillating goes down, and there is no second phase of inflation once $f \lesssim 0.1 M_{\text{pl}}$.

In Fig. 5 we plot the posteriors for f_{NL} for the two different choices of upper bound on f. As discussed in Appendix B, we show results both assuming the standard Horizon Crossing Approximation, and the improved approximation calibrated on numerical calculations. The
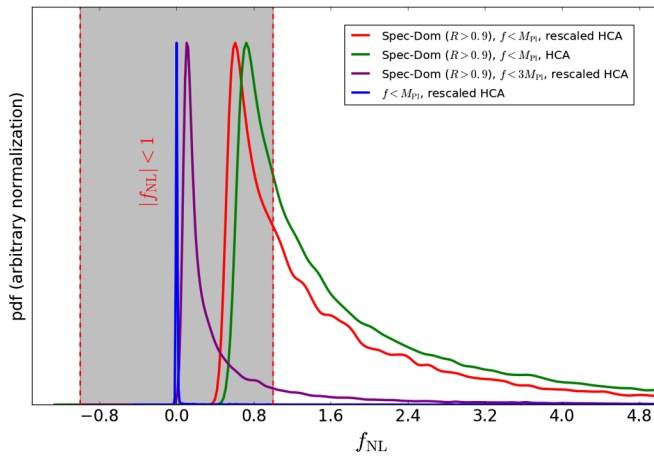
curves for the default prior $f < M_{\text{Pl}}$ are well within the Planck CMB bound, with typical values of f_{NL} of order unity. This is thus within range of future experiments, especially if $\sigma(f_{\text{NL}})$ could be pushed significantly below one.

We can understand the f_{NL} distribution better by noting that, in the fully spectator-dominated limit, cf. Eq. (25),

$$f_{\text{NL}} \approx \frac{5\pi^2}{3f^2}. \qquad (43)$$

The maximum value $f = M_{\text{pl}}$ then corresponds to $f_{\text{NL}} = -0.65$, thus explaining the cutoff in the f_{NL} distribution. This cutoff is smoothed out because we consider the range $R = 0.9$–1 and the expression for f_{NL} above is to be multiplied by R^2. The relation between f and f_{NL} also makes clear that the posterior is dominated by a limited range of f just below and up to the cutoff. Therefore, it is the prior of a sub-Planckian decay constant that pushes us towards $|f_{\text{NL}}| \gtrsim 1$ (assuming the perturbations are dominated by the spectator field in the first place). For the more inclusive prior, $f < 3M_{\text{pl}}$, the typical value of f_{NL} is significantly smaller. The low non-Gaussianity at large f can be understood by noting that in this limit, $V(\chi)$ becomes more and more like a flat, slow-roll potential, which naturally has slow-roll suppressed f_{NL}.

We illustrate the relation between f and f_{NL} in Fig. 6, which shows the joint posterior distribution of f and f_{NL} in the spectator-dominated regime. This figure also clearly illustrates the difference in the dependence of f_{NL} on f between the HCA and the rescaled/improved HCA. Note
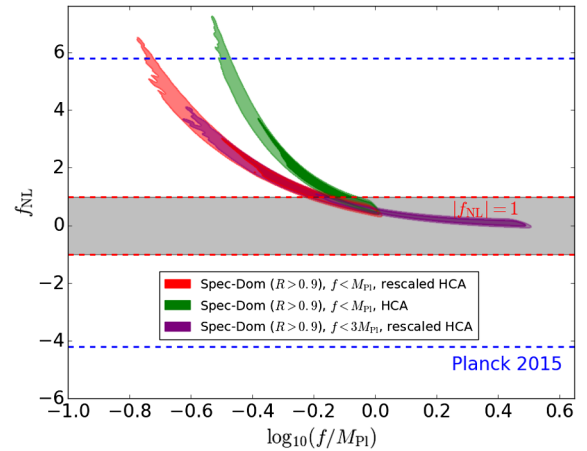
FIG. 5. Posterior distribution of f_{NL} in quadratic-axion scenario (case A), assuming Planck constraints on f_{NL}, n_s and r. The blue curve shows the general f_{NL} distribution in this model, dominated by the inflaton-dominated regime, where $f_{\text{NL}} \approx 0$. In red and green (see main text and Appendix for discussion of the two approaches), we impose the condition that the curvature perturbations are dominated by the spectator χ ($R > 0.9$). In this regime, while the exact shape of the f_{NL} posterior is prior dependent (cf. purple curve), f_{NL} is generically of order unity (58% probability of $|f_{\text{NL}}| > 1$ for our default prior $f < M_{\text{pl}}$, red curve).

FIG. 6. Joint posterior distribution of f_{NL} and "axion decay constant" f in quadratic-axion model. The red (purple) contours show the posterior restricted to the spectator-dominated regime with a prior $f < M_{\text{Pl}}$ ($f < 3M_{\text{Pl}}$). The green contour shows the same, but without the correction factor applied to the HCA prediction. The dashed horizontal lines indicate the current 1σ range from Planck, and the level of the constraints aimed for by future galaxy surveys, $|f_{\text{NL}}| \sim 1$.

however that the main qualitative conclusions are not strongly affected by whether or not the correction factor is applied and are thus not sensitive to the exact details of the approximation used to compute $f_{\rm NL}$.

B. The curvaton

For the curvaton, we find that the spectator-dominated regime is reached for low initial field values χ_* and low ratios $\Gamma_{\rm reh}/m_\chi$, the latter corresponding to a long reheating phase. This is illustrated in Fig. 7, which shows the posterior probability distributions (68 and 95% confidence level) in the spectator-dominated regime ($R > 0.9$). The blue regions include all CMB measurements discussed above, while the unfilled contours are derived without including the Planck $f_{\rm NL}$ measurement.

The spectator-dominated parameter region can be understood as follows. The requirement $N_\chi \gg N_\phi$ can be phrased as [cf. Eqs. (13), (28)],

$$\frac{r_{\chi,{\rm reh}}}{\chi_*} \gg \frac{\phi_*}{m_{\rm Pl}^2}. \tag{44}$$

Since by definition $r_{\chi,{\rm reh}} \leq 1$, we clearly at least need $\chi_*\phi_* \ll m_{\rm Pl}^2$. Assuming this is satisfied, there is in addition the requirement that $r_{\chi,{\rm reh}}$ is not too small. As long as $r_{\chi,{\rm reh}} \ll 1$, it is easy to show that $r_{\chi,{\rm reh}} \sim \chi_*^2\sqrt{m_\chi/\Gamma_{\rm reh}}/m_{\rm Pl}^2$, translating Eq. (44) into the requirement

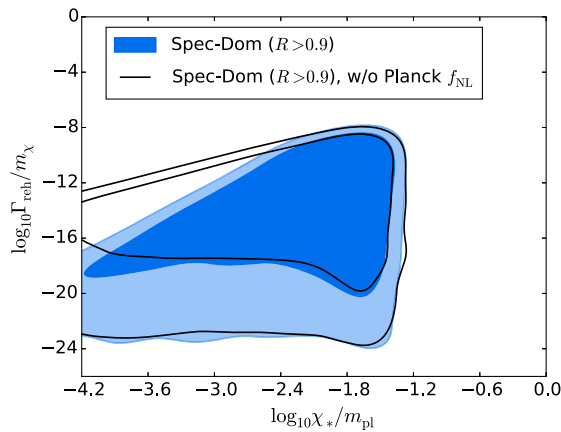$$\frac{\Gamma_{\rm reh}}{m_\chi} \ll \left(\frac{\chi_*}{\phi_*}\right)^2. \tag{45}$$

FIG. 7. Posterior parameter distribution in the spectator-dominated regime of the curvaton model (case B). The black contours show the constraints without the Planck bound on $f_{\rm NL}$, while the blue filled contours show the result with all Planck constraints. For the spectator (i.e. curvaton) to dominate, reheating needs to occur very long after the start of oscillations in the curvaton (extremely low $\Gamma_{\rm reh}/m_\chi$), representing a fine-tuning. The upper bound on $\Gamma_{\rm reh}/m_\chi$ becomes stricter for small initial field values, χ_*, as explained in the text.

Thus, the smaller the value of χ_*, the more the ratio $\Gamma_{\rm reh}/m_\chi$ has to be tuned to extremely small values. In physical terms, we are forced towards low initial field values, but the smaller χ_* is, the smaller the ratio of curvaton to radiation energy density is at the start of the curvaton phase, and thus the longer the curvaton phase needs to last to make the curvaton fraction r_χ non-negligible.

The above explains well the unfilled contours in Fig. 7. The blue regions show that when the Planck $f_{\rm NL}$ bound is added, an additional part of parameter space is excluded. Namely, in the curvaton-dominated regime, and for small $r_{\chi,{\rm reh}}$, we have $f_{\rm NL} \sim r_{\chi,{\rm reh}}^{-1}$ so that the Planck bound forces

$$\frac{\Gamma_{\rm reh}}{m_\chi} \lesssim (f_{\rm NL,max}^{\rm Planck})^2\chi_*^4 \tag{46}$$

(where the 2σ Planck bound is $f_{\rm NL,max}^{\rm Planck} \sim 10$), thus explaining the steeper scaling of the maximum value of $\Gamma_{\rm reh}/m_\chi$ with χ_* in the filled blue regions.

Is the spectator-dominated regime fine-tuned? We have seen above that to satisfy the condition of large R, one needs an extremely large hierarchy between the scales m_χ and $\Gamma_{\rm reh}$, translating to a reheating scale many orders of magnitude below the inflation scale. In this sense, the regime where the spectator/curvaton is important is very fine-tuned. Moreover, we require small initial field values in Planck units. At the same time, we find the posterior probability for, say, $R > 0.5$ vs. $R < 0.5$, to be of the same order[9] The reason for this is that we imposed logarithmic priors on $\Gamma_{\rm reh}$, etc, with very small lower bounds, reflecting the huge hierarchy between the minimum allowed reheating scale (here chosen to be $H_{\rm reh} \sim 10^{-13}$ GeV, corresponding to $T_{\rm reh} \sim 1$ TeV, see Appendix A) and the Hubble scale at the end of inflation, $H_{\rm end} \sim 10^{13}$ GeV. We also find that the posterior distribution of R (not shown) is bimodal, with peaks at $R = 0$ and $R = 1$. This is again a prior driven effect. There is simply a large parameter volume in the regions where either the spectator or inflaton domination conditions are saturated, cf. e.g. Eq. (45), and only an order of magnitude of parameter range in the intermediate regime.

In Fig. 8, we consider the posterior distribution of $f_{\rm NL}$ both in the general model, and in the spectator dominated regime. In the latter case (red), the peak corresponds to the scenario where the curvaton stage lasts long enough for the

---

[9]The probability of being in the spectator-dominated regime is increased somewhat by the upper bound on the tensor-to-scalar ratio, but this is partially an artifact of our choice of a quadratic inflaton potential, which in the inflaton-dominated regime is in tension with the data (one can fit n_s at the cost of too large a value of r). We have considered the more general case of a varying inflaton potential power law index, see Sec. V D, and find that in this case, the probability of being in the spectator-dominated regime is somewhat suppressed compared to the ϕ^2 model.
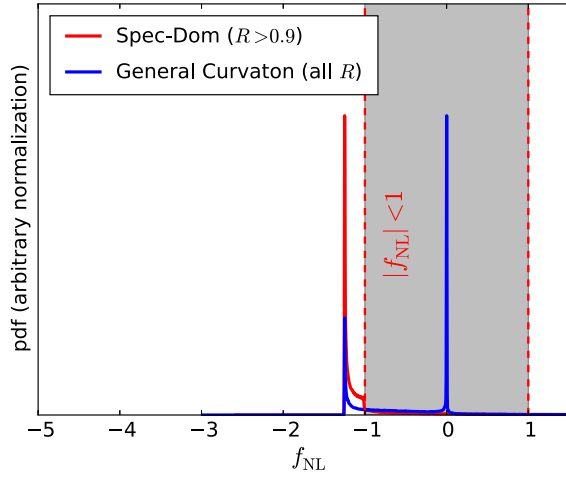
FIG. 8. Posterior distribution on $f_{\rm NL}$ in curvaton scenario (case B), assuming Planck measurements of $f_{\rm NL}$, n_s and r. The blue curve shows the general $f_{\rm NL}$ distribution in this model, while the red curve is restricted to spectator domination, where curvature perturbations are mostly sourced ($R > 0.9$) by the curvaton χ. In this regime, wile the exact shape of the $f_{\rm NL}$ posterior is sensitive to priors, $f_{\rm NL}$ is generically of order unity (79% probability of $|f_{\rm NL}| > 1$). In particular, most of the posterior probability is in the parameter region where the curvaton phase has lasted long enough for the curvaton to dominate the background energy density of the Universe, $r_{\chi,\rm reh} \to 1$, so that the non-Gaussianity reaches its asymptotic level, $f_{\rm NL} \to -5/4$.
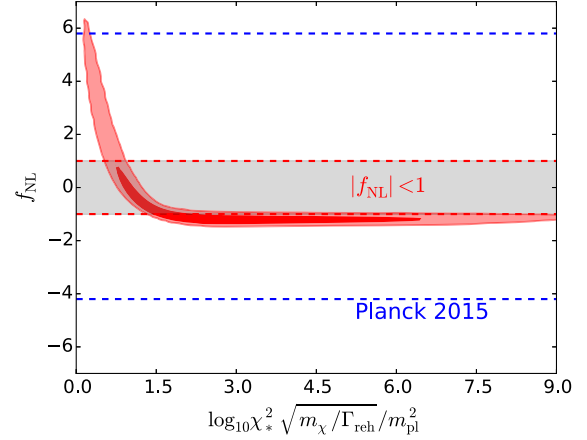

FIG. 9. Posterior distribution of $f_{\rm NL}$ vs combination of model parameters in the curvaton model, restricted to the spectator-dominated regime ($R > 0.9$). The parameter combination $\chi_*^2 \sqrt{m_\chi/\Gamma_{\rm reh}}/m_{\rm Pl}^2$ is approximately equal to the ratio $r_{\chi,\rm reh}$ for low $r_{\chi,\rm reh}$ (whereas large values of $\chi_*^2 \sqrt{m_\chi/\Gamma_{\rm reh}}/m_{\rm Pl}^2$ correspond to $r_{\chi,\rm reh} = 1$), making it a good proxy for $f_{\rm NL}$. The dashed horizontal lines indicate the current 1σ limits from Planck, and the constraints aimed for by future galaxy surveys, $|f_{\rm NL}| \sim 1$.

curvaton to dominate the energy budget of the Universe, $r_{\chi,\rm reh} \to 1$ and $f_{\rm NL} \to -5/4$. We find that 79% of the posterior distribution has $|f_{\rm NL}| > 1$, making future constraints at this level extremely interesting. In particular, $f_{\rm NL} = -5/4$ is clearly an important target.

The dominance of the peak at $f_{\rm NL} = -5/4$ reflects that our priors allow a large parameter volume where $r_{\chi,\rm reh} = 1$ is saturated, i.e. once $\Gamma_{\rm reh}$ is low enough for the curvaton to dominate the background energy, lowering $\Gamma_{\rm reh}$ further by orders of magnitude will maintain $f_{\rm NL} = -5/4$. If we had imposed priors that penalize a large hierarchy between $\Gamma_{\rm reh}$ and m_χ, the results would change, favoring the large negative $f_{\rm NL}$ regime (low $r_{\chi,\rm reh}$) relative to $f_{\rm NL} = -5/4$. Of course, such a change in priors would also make satisfying the condition of large R more manifestly fine-tuned. In the general case (blue curve), we see the aforementioned bimodality of the posterior of R, with the inflaton-dominated regime leading to the single-field value $f_{\rm NL} \approx 0$ and the spectator-dominated case giving $f_{\rm NL} = -5/4$.

Now focusing on the spectator-dominated regime, Fig. 9 shows the joint posterior distribution of $f_{\rm NL}$ with the parameter combination $\chi_*^2 \sqrt{m_\chi/\Gamma_{\rm reh}}/m_{\rm Pl}^2$, which, as explained above, is approximately equal to $r_{\chi,\rm reh}$ for low values of $r_{\chi,\rm reh}$. A future measurement of $f_{\rm NL}$ with order unity precision thus may provide important information on

the curvaton model, and in particular on this parameter combination. In particular, for $f_{\rm NL} \gtrsim -1$, there is a sharp relation between $f_{\rm NL}$ and the above parameter combination. If $f_{\rm NL} \approx -5/4$ is found (and a large fraction of the parameter space gives this result), it would tell us that $\log_{10}(\chi_*^2 \sqrt{m_\chi/\Gamma_{\rm reh}}/m_{\rm Pl}^2) \gtrsim 1.5$. In this regime, $f_{\rm NL}$ unfortunately does not distinguish between different values above this lower bound.

C. Modulated reheating

In the modulated reheating model, the spectator-dominated regime is reached if [cf. Eq. (35)],

$$\left| \frac{\lambda'}{\lambda} \right| \gg \frac{\phi_*}{m_{\rm Pl}^2}, \qquad (47)$$

(the transfer function from χ_* to $\chi_{\rm reh}$ generally has a small effect), corresponding to large λ_1/M_c and/or $\lambda_2 \chi_{\rm reh}/M_c^2$ (most of the weight in the prior distribution of λ_0 lies around values of $\mathcal{O}(10^{-1})$ because of the uniform prior). This region is shown in Fig. 10. The filled contours show the usual confidence regions with the prior $R > 0.9$, including all Planck data discussed, while the solid empty contours represent the same region, but without the $f_{\rm NL}$ bound.

We have also (dashed empty contours) included the posterior in the general model, i.e. without the spectator domination requirement on R (and also without the $f_{\rm NL}$ measurement included), to illustrate that the strong correlation between λ_1/M_c and λ_2/M_c^2 is there regardless of the requirement on R. It is mostly prior driven, and comes from
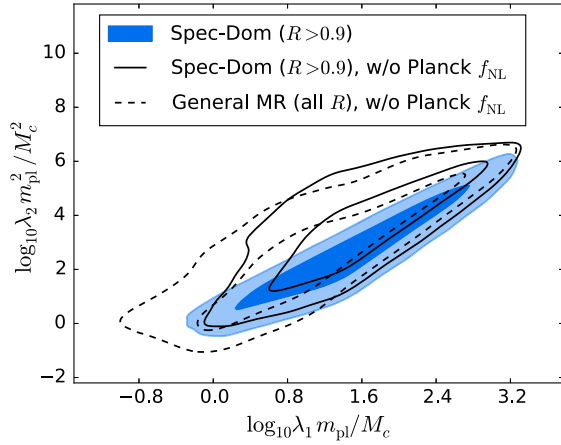
FIG. 10. Spectator-dominated regime ($R > 0.9$) of the modulated reheating model (case C). The contours show the posterior distribution of the first- and second-order coefficients of χ in the inflaton coupling constant determining the reheating decay rate, see Eq. (34). The black dashed contours depict constraints without the Planck bound on $f_{\rm NL}$ for general R. The strong correlation between the two parameters shown is due to the joint dependence on the cutoff mass M_c. The black solid contours additionally require $R > 0.9$. This spectator-dominated regime thus corresponds to strong dependence of λ on χ. The filled blue contours finally add the Planck $f_{\rm NL}$ limit, limiting the final allowed region to lower values of λ_2/M_c^2.

FIG. 11. Posterior distribution of $f_{\rm NL}$ in modulated reheating model (case C), assuming Planck constraints on $f_{\rm NL}$, n_s and r. The blue curve shows the general $f_{\rm NL}$ distribution in the model, while the red curve is restricted to spectator domination ($R > 0.9$), where fluctuations in χ dominate the final curvature perturbations due to their effect on reheating. In the former (general) case, a large fraction of the posterior probablity lies in the inflaton-dominated regime with negligible $f_{\rm NL}$. In the latter case, while the exact shape of the $f_{\rm NL}$ posterior is sensitive to priors, $f_{\rm NL}$ is generically of order unity (72% posterior probability of $|f_{\rm NL}| > 1$), with a broad distribution.

the fact that both quantities scale with the same cutoff mass M_c (and that the dimensionless quantities λ_1 and λ_2 follow uniform priors). What the requirement of spectator domination does is to shift λ_1/M_c and λ_2/M_c^2 to larger values along the correlation direction, as shown by the solid black contours and filled blue regions.

Thus, spectator domination requires an effective cutoff scale M_c not much larger than $\sim 0.1 m_{\rm Pl}$, allowing the effect of χ on λ to be large enough. Since we do not want any contribution to λ to be larger than unity, the requirement of large λ_1/M_c and λ_2/M_c^2 in Planck units does again mean we need small initial field values, $\chi_* \ll m_{\rm Pl}$, which can be considered fine-tuning. For the same reasons discussed in the curvaton case, related to our choice of priors, our chains do give a bimodal distribution of R with peaks of comparable amplitude at $R = 0$ and $R = 1$ despite this fine-tuning.

Figure 11 depicts the posterior distribution of $f_{\rm NL}$ for both the general case and the spectator-dominated case. In the latter case, we see a relatively broad distribution of values (in contrast with the curvaton model), with typical values of order $|f_{\rm NL}| \sim 1$–5 (we note that when we do not implement the current observational bound on $f_{\rm NL}$, the distribution is significantly broader (not shown), with typical values of order $|f_{\rm NL}| \sim 10$–20). We find that 72% of the parameter space in the spectator-dominated regime has $|f_{\rm NL}| > 1$.

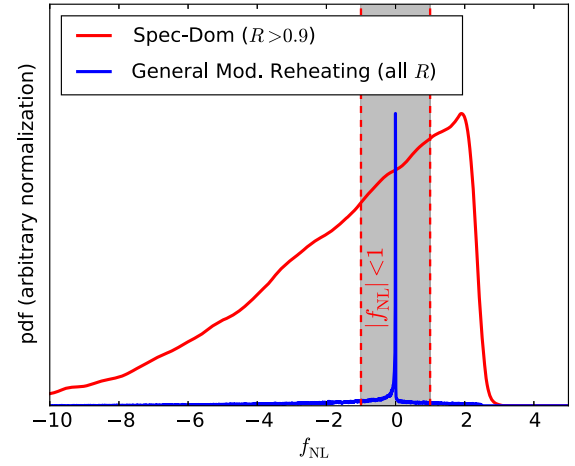The distribution at the lower end has a relatively sharp cutoff. This follows from the specific form of the

expression for $f_{\rm NL}$, Eq. (36). Ignoring the evolution of χ, it reduces to

$$f_{\rm NL} \approx 5\left(1 - \frac{\Gamma''_{\rm reh}\Gamma_{\rm reh}}{(\Gamma'_{\rm reh})^2}\right) = \frac{5}{2}\left(1 - \frac{\lambda''(\chi_{\rm reh})\lambda(\chi_{\rm reh})}{(\lambda'(\chi_{\rm reh}))^2}\right). \quad (48)$$

Since we have chosen the coefficients in the expansion of the reheating coupling to all be positive, this gives an upper bound $f_{\rm NL} < 5/2$. This cutoff gets smoothed out once the evolution of χ is included (the partial derivatives in Eq. (36)), thus explaining the shape of the red curve at the high $f_{\rm NL}$ end.

In the general case (blue), the bimodal distribution of R again leads to a superposition of the inflaton-dominated regime's $f_{\rm NL} \approx 0$ and the broader distribution corresponding to the spectator-dominated regime.

Studying $f_{\rm NL}$ in the spectator-dominated scenario in more detail, Fig. 12 shows the joint posterior of $f_{\rm NL}$ and $\lambda_2\lambda_0/\lambda_1^2$. This parameter combination mostly determines $f_{\rm NL}$ in the spectator-dominated regime if λ' is dominated by the λ_1 contribution and λ by λ_0, cf. Eq. (48). A measurement of $f_{\rm NL}$ provides information on the modulated reheating parameter space and in particular on this combination of parameters describing the coupling of the inflaton to χ and to the particles into which it reheats.

In summary, while the physics behind the mechanisms is very different, the modulated reheating has similar phenomenology to the curvaton scenario. The main qualitative
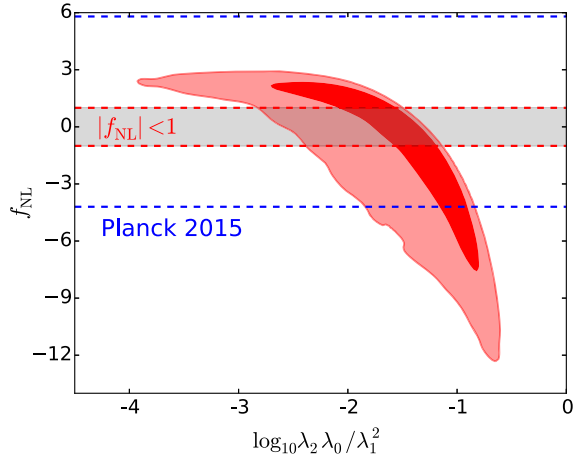
FIG. 12. Joint posterior distribution of f_{NL} and a combination of parameters describing the inflaton reheating decay rate and its dependence on the field χ, assuming spectator domination ($R > 0.9$). A measurement of f_{NL} provides valuable information on the modulated reheating process, and in particular the quantity $\lambda_2\lambda_0/\lambda_1^2$, cf. Eq. (36). The dashed horizontal lines indicate the current 1σ limits from Planck, and the constraints aimed for by future galaxy surveys, $|f_{NL}| \sim 1$.
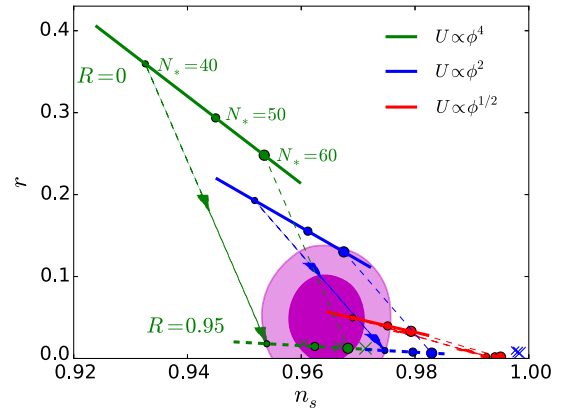

FIG. 13. Phenomenology in the (n_s, r) plane of models with power-law inflaton potentials, extended beyond the single-field case into the spectator domain ($R > 0$). Magenta contours show current Planck constraints. Solid lines show predictions for inflaton-dominated models ($R = 0$, equivalent to single-field). N_* is the number of e-folds to the end of inflation. The arrows connect the $R = 0$ regime to the spectator-dominated regime (here, $R = 0.95$, shown in dashed). This is for the common case of $\eta_*^\chi \approx 0$, while crosses indicate the alternative of large η_*^χ. Otherwise ruled out inflaton potentials, such as $U(\phi) \propto \phi^4$ become viable again in the spectator-dominated regime.

difference is that for spectator-dominated modulated reheating, the f_{NL} distribution does not peak at a special value ($f_{NL} = -5/4$ for the curvaton). Instead, it has a broader distribution, with a "smooth" cutoff around $f_{NL} \sim 5/2$.

D. Observational prospects

Spectator models are a relatively simple extension of single-field inflation, which itself can be seen as the inflaton-dominated corner of spectator model parameter space. Regarding the inflaton potential, $U(\phi)$, we have so far focused on the simple quadratic potential because predictions for f_{NL} are rather robust against the details of the inflaton potential. Technically, however, to fit n_s and r well with realistic values of the number of e-folding before the end of inflation, more freedom in the shape of the inflaton potential is needed. In particular, let us consider the class of power-law models,

$$U(\phi) \propto \phi^n, \qquad (49)$$

where we will allow noninteger values of n.

Figure 13 shows the predictions for such models in the (n_s, r) plane, compared to the Planck constraint. The solid lines show the well known single-field/inflaton-dominated ($R = 0$) case, cf. e.g. Fig. 12 in [93]. The dots indicate the number of e-folds before the end of inflation, N_*. As is well known, the Planck data are already in significant tension with the inflaton-dominated quadratic model, but lower powers, e.g. $U \propto \phi^{2/3}$ are in reasonable agreement.

The effect of curvature perturbations more and more generated by the spectator field, i.e. increasing R, is

indicated by the arrows, leading to the mostly spectator-dominated scenarios ($R = 0.95$) shown in dashed lines, cf. Eq. (15). Note that for a given R and a given inflaton potential, n_s does not generally have a fixed value because it still depends on η_*^χ. However, we find that the regime with negligible η_*^χ contribution often dominates so that we chose $\eta_*^\chi = 0$ in this plot. To indicate the range of effects from nonzero η^χ, the crosses show (n_s, r) for the maximum (positive) η_*^χ consistent with the requirement that the spectator field is slowly rolling until after the end of inflation.

Figure 13 thus visualizes that, as the spectator field becomes more important, r goes down, making it easier to evade the tensor-mode constraint, and n_s shifts to larger values. This means that: (1) models that are currently a decent fit in the inflaton-dominated regime (low n power laws) become poor fits in the spectator-dominated case and (2) models with larger power law indices, ruled out by Planck data in the single-field case, become viable again in the spectator-dominated scenario.

We illustrate this for the curvaton model in Fig. 14 (top), which shows the same curves, but in a zoomed-in region. Here, we add the results of MCMC simulations, as above but now treating the power law index n as an additional free parameter with $n = [1/2, 4]$ and requiring $N_* = [46, 58]$. The colored points show the inflaton-dominated posterior region ($R < 0.1$) and the spectator-dominated one ($R > 0.9$). Colors indicate the potential power law index, confirming the picture described above, with the inflaton/spectator-dominated regimes preferring small/large values of n.
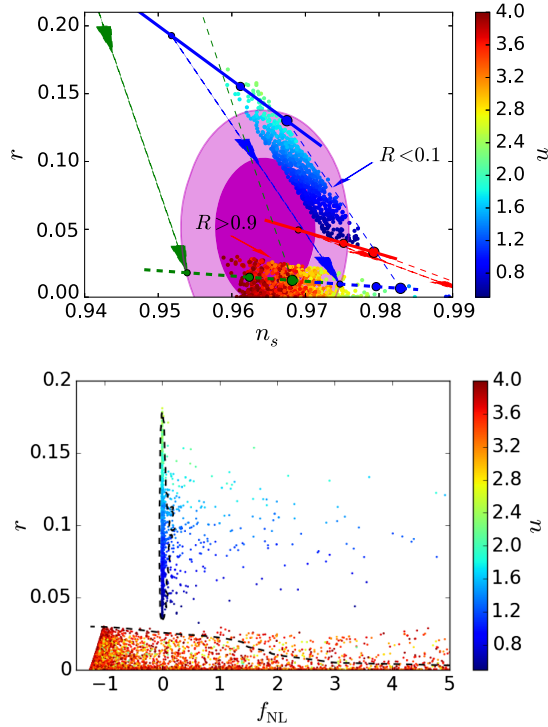
FIG. 14. *Top:* As Fig. 13 (different scale and omitting labels), but with results from MCMC analysis of curvaton model (case B) added in. Here, the power law index n of the inflaton potential is treated as a free parameter and indicated by color. The two sets of points from the Monte Carlo chains correspond to inflaton domination ($R < 0.1$, blue) and spectator domination ($R > 0.9$, yellow-red). The former prefer a low index ($n \approx 0.5–1$) as in the single-field case, while the latter prefer a large index ($n \approx 3–4$). *Bottom:* For the same two regimes ($R < 0.1$ and $R > 0.9$), now we show samples with f_{NL} instead of n_s on the horizontal axis (dashed lines outline the 95% C.L. regions). While the spectator-dominated regime suppresses r, it leads to potentially detectable f_{NL}.

A major difference between the two regimes is that, while in the inflaton-dominated case, r is always within reach of upcoming B-mode searches (assuming a power law potential), for $R \to 1$, one can obtain r arbitrarily close to zero while perfectly fitting n_s, cf. Eq. (16). This is where primordial non-Gaussianity comes in, as illustrated in the bottom panel of Fig. 14. While in the (fully) inflaton-dominated regime, the single-field consistency condition effectively sets f_{NL} to zero (the outlying blue points with non-negligible f_{NL} are explained by their spectator contribution, i.e. $R \sim 0.1$ and $N_{\chi_*\chi_*}/N_{\chi_*}^2$ very large), the spectator-dominated regime typically generates $|f_{NL}| \gtrsim 1$. The same is true for the other two models considered in this paper. The fact that r is typically large in the inflaton-dominated regime is specific to large-field potentials, such as the power laws chosen here. For different types of potentials, it is possible to have small r even in the single-field/inflaton-dominated regime.

In summary, for inflaton-dominated models, f_{NL} is small and out of reach of near-future experiments, but r is large (assuming a power law inflaton), while in spectator-dominated models, values of f_{NL} within the scope of upcoming surveys are common, but r is suppressed (we do note that, while in the latter case, large f_{NL} is expected, it is not impossible to be in the worst-case scenario where both r and f_{NL} are negligibly small). Thus, in order to unravel the mysteries of inflation, it is crucial for future probes to aim their sights at both tensor fluctuations and primordial non-Gaussianity.

VI. DISCUSSION AND CONCLUSIONS

Upcoming galaxy surveys aim to significantly improve constraints on local primordial non-Gaussianity, from the current Planck bound $f_{NL} = 0.8 \pm 5.0$, to constraints with uncertainties $\sigma(f_{NL}) \lesssim 1$. Motivated by this prospect, we have here derived current constraints on a range of multi-field inflation models given Planck CMB data and physically motivated parameter priors, and compared the resulting predicted values of f_{NL} to the expected future constraints. Our goal was to obtain quantitative estimates, given an inflationary model, of the discovery potential of local non-Gaussianity with these future surveys, and to quantify what such a future f_{NL} may teach us about the physics behind inflation.

We have specifically focused on so-called spectator models, where, while inflation is driven by the inflaton field, the primordial curvature perturbations are partially or fully generated by a second field, the "spectator". At horizon exit, this spectator field does not contribute to the curvature perturbations, but its perturbations can be converted into curvature perturbations afterward through super-horizon evolution. We have considered three specific mechanisms for this process with the conversion occurring during different phases: (A) during or after inflation before either field has decayed into radiation, (B) after inflation while the inflaton has already decayed into radiation and the spectator (i.e. curvaton) oscillates around the minimum of its potential, and (C) after inflation during the reheating process itself.

If the relative contribution of the spectator field to the final primordial curvature power spectrum is close to one, significant non-Gaussianity can be generated, which is why our main focus has been on this set of "spectator-dominated" models. While there are significant differences between the three scenarios (A)–(C), we will below discuss some of the main general conclusions.

Typically, to be in the spectator-dominated regime, some form of fine-tuning is required. For instance, in all three scenarios, small values of the initial spectator field value are needed. One might wonder if this tuning leads to problems with the classical description of the background evolution, due to stochastic quantum fluctuations in the field. However, as discussed in Appendix A, we have

throughout the paper explicitly restricted the analysis to field values much larger than the amplitude of the quantum fluctuations ($\delta\chi_* \sim \delta\phi_* \sim H_*/2\pi \sim 10^{-5} m_{\rm Pl}$ for large-field inflaton potentials) so that quantum effects are guaranteed to be negligible even for the small field values required to be in the spectator-dominated regime. An additional example of apparent fine-tuning is that, in the curvaton scenario, the reheating scale needs to be tuned to be many orders of magnitude below the scale of inflation and the curvaton mass, corresponding to extremely late reheating (although not in clear tension with data). On the other hand, statements about fine-tuning are always strongly prior dependent. For example, since our MCMC analysis employed wide, logarithmic prior ranges on most dimensionful parameters, we found in both scenarios (B) and (C) that being in the spectator-dominated regime is approximately equally likely as the alternative. However, this does not remove the objection that large hierarchies between parameters may be unnatural from a model building perspective. Such theory-based prejudice could have been incorporated by modifying our priors, but we chose not to pursue this here.

Assuming spectator domination ($R > 0.9$), we have quantified the posterior distribution of $f_{\rm NL}$ given current Planck data for each of the three scenarios. We have quantified the promise of next-generation $f_{\rm NL}$ measurements by quoting the posterior probability of $|f_{\rm NL}| > 1$, which we will summarize below. Assuming $|f_{\rm NL}| > 1$ can be distinguished from zero at sufficient significance, this gives the probability of detection of non-Gaussianity. Conversely, if an upper bound $|f_{\rm NL}| < 1$ is obtained from the data, the posterior probability of exceeding $|f_{\rm NL}| = 1$ tells us what fraction of the currently allowed parameters space will be ruled out. However, the above quantity does not tell the full story[10] so below we also quote what fraction of the posterior distribution obtained *without* including the Planck $f_{\rm NL}$ bound has $|f_{\rm NL}| > f_{\rm NL,max}^{\rm Planck} = 10$ (corresponding approximately to the 2σ Planck bound) and what fraction has $|f_{\rm NL}| > 1$.

(i) **Case A-Quadratic-axion**
With Planck $f_{\rm NL}$: $P(|f_{\rm NL}| > 1) = 58\%$
Without: $P(|f_{\rm NL}| > 1(10)) = 63(6)\%$

(ii) **Case B-Curvaton**
With Planck $f_{\rm NL}$: $P(|f_{\rm NL}| > 1) = 79\%$
Without: $P(|f_{\rm NL}| > 1(10)) = 83(14)\%$

(iii) **Case C-Modulated reheating**
With Planck $f_{\rm NL}$: $P(|f_{\rm NL}| > 1) = 72\%$
Without: $P(|f_{\rm NL}| > 1(10)) = 92(60)\%$

We see that in the modulated reheating scenario, the Planck $f_{\rm NL}$ constraint has already ruled out a significant fraction of the parameter space allowed without taking PNG into account, but that in the other cases we are only just starting to take advantage of $f_{\rm NL}$. While, as we have discussed, the numbers above are prior dependent (especially in case A, which relies on the maximum value of the decay constant f being of order $M_{\rm Pl}$), they suggest that, if inflation is described by one of these models where the curvature perturbations are generated by a field other than the inflaton, future $f_{\rm NL}$ searches with $\sigma(f_{\rm NL}) \lesssim 1$ have a good shot at a detection and will probe these models well beyond the current Planck $f_{\rm NL}$ constraint.

If a detection of $f_{\rm NL}$ *is* achieved, the most important implication would of course be the discovery of multifield inflation (although there are caveats to the single-field consistency conditions that allow non-zero $f_{\rm NL}$ in certain special single-field scenarios [11,12]). In addition, we have shown that a measurement of $f_{\rm NL}$ in the context of the models above also tells us about the values of certain parameter combinations, thus providing hints about the nature of the multifield model describing the early Universe. We have also highlighted the complementarity between B-mode searches constraining primordial tensor perturbations and measurements of galaxies and the CMB constraining primordial non-Gaussianity. It is such a multipronged approach that provides the best opportunity for improving our understanding of the physics of the extremely early Universe.

In conclusion, while large or order unity $f_{\rm NL}$ is *not* a general prediction of multifield inflation, it appears to be quite generic in spectator-dominated models. Arguably, these are the more interesting multifield models regardless of $f_{\rm NL}$, as the case where the primordial fluctuations are fully determined by the inflaton field is phenomenologically indistinguishable from single-field models. The appearance of order unity $f_{\rm NL}$ in spectator-dominated and similar models has been highlighted many times in the literature, but here we have sampled the full parameter space of a range of models, taking into account observational constraints, leading to a more comprehensive quantitative assessment of the typical prediction for $f_{\rm NL}$ and of the spectator multifield phenomenology in general.

ACKNOWLEDGMENTS

---

[10]Since by default we included the Planck bound on $f_{\rm NL}$ to compute the posterior, some caution is needed in interpreting the posterior probability of getting $|f_{\rm NL}| > 1$. If the $f_{\rm NL}$ posterior *without* including the $f_{\rm NL}$ bound from Planck is very wide compared to $\sigma(f_{\rm NL})$ from Planck, the default posterior *with* the Planck $f_{\rm NL}$ bound included is essentially determined by $\sigma(f_{\rm NL}) \sim 5$, and saying that a bound with $\sigma(f_{\rm NL}) \lesssim 1$ rules out a large part of currently allowed parameter space is equivalent to the trivial statement that the future error bars are smaller than the current ones. In this scenario, it could be that the Planck $f_{\rm NL}$ bound had already ruled out an overwhelming fraction of the previously allowed parameter space, and a future tighter bound will simply rule out a little bit more. Therefore, it is also important to quantify how much better a future $f_{\rm NL}$ constraint does than the current CMB bound.

APPENDIX A: PARAMETERS AND PRIORS

In this Appendix, we consider parameter priors and other constraints assumed in the MCMC likelihood analysis. For each model, there is a set of basic parameter priors, given in Tables I–III. On top of these priors, various additional constraints, other than those from the data discussed in the main text, are imposed. There can be significant redundancy in these priors and constraints, i.e. they are not all independent. Let us first consider requirements that are imposed on all three models.

(i) First of all, we always demand the spectator definition given in Eq. (13) is satisfied. Secondly, we require all four slow-roll parameters at t_* to be small,

$$\epsilon_*^\phi, \epsilon_*^\chi, |\eta_*^\phi|, |\eta_*^\chi| < 0.1. \qquad (A1)$$

(ii) Moreover, for a classical treatment of the spectator field to be appropriate, we require that its initial value is much larger than the initial quantum fluctuations,

$$\chi_* > 10 \times \delta\chi_* = 10 \times \frac{H_*}{2\pi} \qquad (A2)$$

(we use a fixed value $H_* = 4 \times 10^{-5} m_{\rm Pl}$).

(iii) Unless otherwise noted, we apply logarithmic priors to dimensionful parameters (and parameters that were dimensionful before dividing out powers of m_ϕ).

(iv) We will define the spectator-dominated regime by the somewhat arbitrary threshold,

$$R > 0.9. \qquad (A3)$$

Let us now consider the specific parameters and priors/constraints for each model.

1. Priors case A: Quadratic-axion

(i) The parameters sampled in the MCMC and their default prior ranges are given in Table I.

(ii) As already incorporated there, we assume by default that the decay constant is sub-Planckian

$$f < M_{\rm Pl} \qquad (A4)$$

(note that this is the Planck mass, not the reduced Planck mass), although we explicitly study how the results depend on the upper bound.

TABLE I. Parameters and default priors for case A: the quadratic-axion model. Additional constraints on the parameters are described in the text.

Param.	Description	Prior
V_0/m_ϕ^2	spectator amplitude	$[10^{-52} m_{\rm Pl}^2, 10^5 m_{\rm Pl}^2]$ (log)
f	spectator "decay constant"	$[10^{-4} m_{\rm Pl}, M_{\rm Pl}]$ (log)
χ_*/f	spectator initial phase	$[0, 1/2]$ (linear)
ϕ_*	inflaton initial field	$[10 m_{\rm Pl}, 30 m_{\rm Pl}]$ (log)

TABLE II. Parameters and default priors for case B: The curvaton model. Additional constraints on the parameters are described in the text.

Param.	Description	Prior
m_χ/m_ϕ	spectator mass	$[10^{-26}, 1]$ (log)
$\Gamma_{\rm reh}/m_\phi$	spectator reheating rate	$[10^{-26}, 1]$ (log)
χ_*	spectator initial field	$[10 \times H_*/2\pi, m_{\rm Pl}]$ (log)
ϕ_*	inflaton initial field	$[3 m_{\rm Pl}, 35 m_{\rm Pl}]$ (log)

(iii) We impose a linear prior on χ_*/f because in axion models, this quantity arises as a random phase.

(iv) The lower bound on V_0/m_ϕ^2 is derived from the requirement that reheating occurs at an energy $\rho_{\rm reh} = 3 m_{\rm Pl}^2 H_{\rm reh}^2 > (10^3 \text{ GeV})^4$ (cf. [93]), i.e. before the electroweak phase transition, and that before that time the constant-ζ phase is reached where both fields are oscillating around their potential minima (see Fig. 1). Since the spectator/axion starts rolling approximately[11] when its mass m_χ, given by Eq. (26), exceeds the Hubble scale H, we obtain an order-of-magnitude lower bound (assuming $m_\phi \sim 10^{13}$ GeV) of $(V_0/m_\phi^2)_{\rm min} = 10^{-52} m_{\rm Pl}^2$.

2. Priors case B: Curvaton

(i) The parameters sampled in the MCMC and their default prior ranges are given in Table II.

(ii) The curvaton scenario under consideration requires

$$m_\phi > m_\chi > \Gamma_{\rm reh}. \qquad (A5)$$

(iii) As discussed in the main text, we require the curvaton to be subdominant up to $t_{\rm curv}$,

$$\frac{1}{2} m_\chi^2 \chi_{\rm curv}^2 \ll 3 m_\chi^2. \qquad (A6)$$

(iv) Finally, we have determined the minimum value of $\Gamma_{\rm reh}$ in Table I as in case A, requiring $\rho_{\rm reh} > (10^3 \text{ GeV})^4$. This leads to the prior,

---

[11]We have confirmed the dependence of the time χ starts rolling on V_0 numerically.

TABLE III. Parameters and default priors for case C: the modulated reheating model. Additional constraints on the parameters are described in the text.

Param.	Description	Prior
m_χ/m_ϕ	spectator mass	$[10^{-26}, 1]$ (log)
λ_0	reheating coupling parameter	$[0, 1/2]$ (linear)
λ_1	reheating coupling parameter	$[0, 1]$ (linear)
λ_2	reheating coupling parameter	$[0, 1]$ (linear)
M_c	reheating cutoff parameter	$[10 \times H_*, m_{\rm Pl}]$ (log)
χ_*	spectator initial field	$[10 \times H_*/2\pi, m_{\rm Pl}]$ (log)
ϕ_*	inflaton initial field	$[3m_{\rm Pl}, 35m_{\rm Pl}]$ (log)

$$\frac{\Gamma_{\rm reh}}{m_\phi} > 10^{-26}. \qquad (A7)$$

3. Priors case C: Modulated reheating

(i) The parameters sampled in the MCMC and their default prior ranges are given in Table III.

(ii) The specific scenario under consideration corresponds to the requirement,

$$m_\phi > \Gamma_{\rm reh}(\chi_{\rm reh}) > m_\chi. \qquad (A8)$$

(iii) We also impose

$$\frac{m_\chi}{m_\phi} > 10^{-26}, \qquad (A9)$$

which ensures reheating takes place before the electroweak phase transition (because $\Gamma_{\rm reh} > m_\chi$).

(iv) We require the coupling constant, Eq. (32), and its individual contributions to be significantly smaller than one[12] (to rule out cases where the individual terms are large but cancel due to opposite signs),

$$|\lambda| < 1/2, \qquad |\lambda_1|\frac{\chi_*}{M_c} < 1/2,$$

$$\frac{1}{2}|\lambda_2|\left(\frac{\chi_*}{M_c}\right)^2 < 1/2. \qquad (A10)$$

(v) Finally, as already included in Table III, we demand that the cutoff M_c is significantly above the Hubble scale at t_*,

$$M_c > 10 \times H_*. \qquad (A11)$$

---

[12]This does not ensure that non-perturbative effects are unimportant in the reheating process, but simply that the coupling constant is small enough for the leading-order perturbation theory expression for $\Gamma_{\rm reh}$ to be valid. In addition to this, there may well be non-perturbative effects even for small λ, such as resonant particle production from the vacuum.

In practice, we incorporate M_c into redefinitions of λ_1 and λ_2 and marginalize M_c out analytically.

APPENDIX B: TESTING THE HORIZON CROSSING APPROXIMATION

We discuss here the accuracy of the Horizon Crossing Approximation for computing the curvature perturbations and $f_{\rm NL}$ in the quadratic-axion model. To do so, we numerically compute $f_{\rm NL}$ in the δN formalism using the full equations of motion, i.e.

$$\ddot{\phi} + 3H\dot{\phi} + U_\phi = 0$$
$$\ddot{\chi} + 3H\dot{\chi} + V_\chi = 0$$
$$3m_{\rm Pl}^2 H^2 = \frac{1}{2}\dot{\phi}^2 + \frac{1}{2}\dot{\chi}^2 + U(\phi) + V(\chi). \qquad (B1)$$

We compute the number of e-folds N to a constant energy density hypersurface at a time when both fields have started oscillating around their minima, so that ζ has become constant. From there, one can get the numerical derivatives of N and compute $f_{\rm NL}$ using Eq. (12).

As discussed in the main text, if we do not impose the spectator domination condition, the posterior is dominated by points in parameter space where χ_*/f is not tuned to be small, so that the inflaton dominates the final perturbations
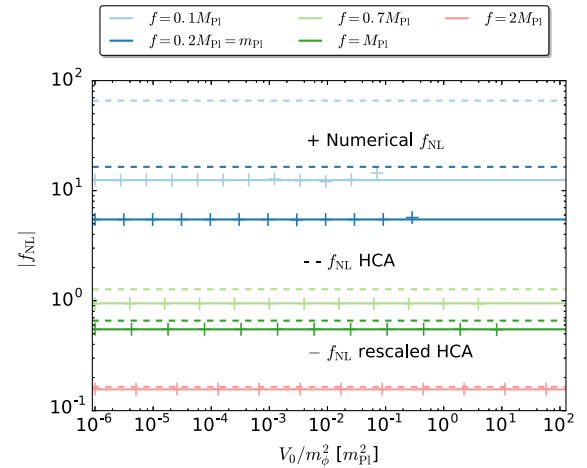

FIG. 15. Comparison of different approaches to calculating $f_{\rm NL}$ in the quadratic-axion model (case A). We show $|f_{\rm NL}|$ as a function of V_0/m_ϕ^2 using the horizon crossing approximation (dashed lines), the HCA with f-dependent correction factor (straight lines) and the full numerical calculation in the δN formalism (+). Results are computed in the limit $\chi_*/f \to 0$ (see text) and we restrict the numerical computation to the range of V_0/m_ϕ^2 values relevant for our likelihood analysis ($|\eta_*^\chi| < 0.1$). While accurate at large f, the HCA is only correct to order-of-magnitude level precision for f significantly below $M_{\rm Pl}$. We have used the numerical calculations to construct an f-dependent rescaling function that brings the HCA prediction in good agreement with the exact result.

and $f_{\rm NL} \approx 0$. Our main region of interest for testing the HCA is thus the regime where we explicitly impose the spectator domination condition,

$$\frac{\chi_*}{f} < \frac{f}{3\pi^2 \phi_*}. \tag{B2}$$

This condition in turn favors larger values of f as they leave a larger range of initial field values that satisfy the above requirement. We thus mainly want to test the HCA for models with f within, say, an order of magnitude from the cutoff, i.e. f close to the Planck scale $M_{\rm pl}$.

In Fig. 15, we show $f_{\rm NL}$ as a function of the amplitude of the axion potential, V_0/m_ϕ^2, for various values of f in the range motivated above. For each parameter choice, we find that $f_{\rm NL}$ converges as $\chi_*/f \to 0$ and in the plot we have chosen values $\chi_*/f \ll f/(3\pi^2\phi_*)$ such that convergence has been reached. The results are minimally sensitive to the choice of ϕ_*.

For large values of f, the HCA (dashed lines) is a reasonably good approximation to the exact numerical results (plus signs). For smaller f however, the HCA systematically overpredicts $f_{\rm NL}$. For comparison, $|f_{\rm NL}| < 5$ (cf. Fig. 5) corresponds to $f \gtrsim 0.4M_{\rm pl}$, between the blue and light green results in Fig. 15. In order to account for the

difference between the HCA and exact result, we implemented a simple function of f that rescales $f_{\rm NL}$ to make it agree with the numerical results. We show the new $f_{\rm NL}$ with this correction factor in solid lines. With the correction factor included, the agreement is quite good, except at high V_0/m_ϕ^2 and low f (again, the low f regime is less relevant in our MCMC analysis). We note that the results do depend also on χ_*/f. While here we have shown the results in the low $\chi_*/f \to 0$ limit, for values of χ_*/f that marginally satisfy Eq. (B2), we find a deviation from the results plotted here. However, the results are always within the range set by the HCA approximation (dashed) and the HCA approximation modified with the correction factor (solid). In our likelihood analysis, to bracket the range of $f_{\rm NL}$ values, we have considered results using either prescription.

We have also looked at how other quantities, such as n_s, r and R are different when using the full equations. Those differences are much smaller, and if the HCA values are within the Planck constraints, so are the ones from the full equations. Moreover, since our main focus is primordial non-Gaussianity, the specifics of those other parameters are of lesser importance to our analysis. Indeed, as we mentioned before, they could be adjusted by a different choice of potential for the inflaton.

---

[1] A. A. Starobinsky, A new type of isotropic cosmological models without singularity, Phys. Lett. B **91**, 99 (1980).

[2] A. H. Guth, Inflationary universe: A possible solution to the horizon and flatness problems, Phys. Rev. D **23**, 347 (1981).

[3] A. D. Linde, A new inflationary universe scenario: A possible solution of the horizon, flatness, homogeneity, isotropy, and primordial monopole problems, Phys. Lett. B **108**, 389 (1982).

[4] A. Albrecht and P. J. Steinhardt, Cosmology for grand unified theories with radiatively induced symmetry breaking, Phys. Rev. Lett. **48**, 1220 (1982).

[5] P. Svrcek and E. Witten, Axions in string theory, J. High Energy Phys. 6 (2006) 051.

[6] S. Dimopoulos, S. Kachru, J. McGreevy, and J. G. Wacker *et al.*, N-flation, J. Cosmol. Astropart. Phys. 8 (2008) 003.

[7] D. Baumann and L. McAllister, Inflation and string theory, 2015, http://adsabs.harvard.edu/abs/2015ist..book.....B.

[8] E. Komatsu and D. N. Spergel, Acoustic signatures in the primary microwave background bispectrum, Phys. Rev. D **63**, 063002 (2001).

[9] J. M. Maldacena, Non-Gaussian features of primordial fluctuations in single-field inflationary models, J. High Energy Phys. 05 (2003) 013.

[10] P. Creminelli and M. Zaldarriaga, Single field consistency relation for the 3-point function, J. Cosmol. Astropart. Phys. 10 (2004) 006.

[11] X. Chen, H. Firouzjahi, M. H. Namjoo *et al.*, A single field inflation model with large local non-Gaussianity, Eurphys. Lett. **102**, 59001 2013).

[12] S. Mooij and G. A. Palma, Consistently violating the non-Gaussian consistency relation, J. Cosmol. Astropart. Phys. 11 (2015) 025.

[13] C. T. Byrnes and K.-Y. Choi, Review of local Non-Gaussianity from multifield inflation, Adv. Astron. **2010** (2010) 724525.

[14] Planck Collaboration, P. A. R. Ade, N. Aghanim *et al.*, Planck 2015 results. XVII. Constraints on primordial non-Gaussianity, Astron. Astrophys. **594**, A17 (2016).

[15] M. Alvarez *et al.*, Testing inflation with large scale structure: connecting hopes with reality, arXiv:1412.4671.

[16] N. Dalal, O. Doré, D. Huterer, and A. Shirokov, The imprints of primordial non-gaussianities on large-scale structure: scale dependent bias and abundance of virialized objects, Phys. Rev. D **77**, 123514 (2008).

[17] S. Matarrese and L. Verde, The effect of primordial non-Gaussianity on halo bias, Astrophys. J. Lett. **677**, L77 (2008).

[18] A. Slosar, C. Hirata, U. Seljak, S. Ho, and N. Padmanabhan, Constraints on local primordial non-Gaussianity from large scale structure, J. Cosmol. Astropart. Phys. 8 (2008) 031.

[19] V. Desjacques and U. Seljak, Primordial non-Gaussianity from the large-scale structure, Classical Quantum Gravity **27**, 124011 (2010).

[20] O. Doré, J. Bock, M. Ashby *et al.*, Cosmology with the SPHEREX All-Sky Spectral Survey, arXiv:1412.4872.

[21] O. Dor *et al.*, Science impacts of the SPHEREx All-Sky Optical to Near-Infrared Spectral Survey: Report of a community workshop examining extragalactic, galactic, stellar and planetary science, arXiv:1606.07039.

[22] http://spherex.caltech.edu/.

[23] P. A. Abell, J. Allison *et al.* (LSST Science Collaboration), LSST Science Book, Version 2.0 arXiv:0912.0201.

[24] R. Laureijs, J. Amiaux, S. Arduini *et al.*, Euclid Definition Study Report, arXiv:1110.3193.

[25] K. N. Abazajian, P. Adshead, Z. Ahmed *et al.*, CMB-S4 Science Book, First Edition, arXiv:1610.02743.

[26] R. de Putter and O. Doré, Designing an Inflation Galaxy Survey: how to measure $\sigma(f_{NL}) \sim 1$ using scale-dependent galaxy bias, arXiv:1412.3854.

[27] S. Ferraro and K. M. Smith, Using large scale structure to test multifield inflation, Phys. Rev. D **91**, 043506 (2015).

[28] D. Yamauchi, K. Takahashi, and M. Oguri, Constraining primordial non-Gaussianity via a multitracer technique with surveys by Euclid and the Square Kilometre Array, Phys. Rev. D **90**, 083520 (2014).

[29] J. Gleyzes, R. de Putter, D. Green *et al.*, Biasing and the search for primordial non-Gaussianity beyond the local type, J. Cosmol. Astropart. Phys. 4 (2017) 002.

[30] C. T. Byrnes, K.-Y. Choi, and L. M. H. Hall, Conditions for large non-Gaussianity in two-field slow-roll inflation, J. Cosmol. Astropart. Phys. 10 (2008) 008.

[31] A. Linde and V. Mukhanov, Non-Gaussian isocurvature perturbations from inflation, Phys. Rev. D **56**, R535 (1997).

[32] T. Moroi and T. Takahashi, Cosmic density perturbations from late decaying scalar condensations, Phys. Rev. D **66**, 063501 (2002).

[33] D. H. Lyth, C. Ungarelli, and D. Wands, Primordial density perturbation in the curvaton scenario, Phys. Rev. D **67**, 023503 (2003).

[34] D. H. Lyth and D. Wands, Generating the curvature perturbation without an inflaton, Phys. Lett. B **524**, 5 (2002).

[35] K. Enqvist and M. S. Sloth, Adiabatic CMB perturbations in pre—big bang string cosmology, Nucl. Phys. **B626**, 395 (2002).

[36] G. Dvali, A. Gruzinov, and M. Zaldarriaga, A new mechanism for generating density perturbations from inflation, Phys. Rev. D **69**, 023505 (2004).

[37] L. Kofman, Probing string theory with modulated cosmological fluctuations, arXiv:astro-ph/0303614.

[38] F. Bernardeau, L. Kofman, and J.-P. Uzan, Modulated fluctuations from hybrid inflation, Phys. Rev. D **70**, 083004 (2004).

[39] G. Dvali, A. Gruzinov, and M. Zaldarriaga, New mechanism for generating density perturbations from inflation, Phys. Rev. D **69**, 023505 (2004).

[40] M. Zaldarriaga, Non-Gaussianities in models with a varying inflaton decay rate, Phys. Rev. D **69**, 043508 (2004).

[41] F. Bernardeau, L. Kofman, and J.-P. Uzan, Modulated fluctuations from hybrid inflation, Phys. Rev. D **70**, 083004 (2004).

[42] D. H. Lyth, Generating the curvature perturbation at the end of inflation, J. Cosmol. Astropart. Phys. 11 (2005) 006.

[43] Q.-G. Huang, A geometric description of the non-Gaussianity generated at the end of multi-field inflation, J. Cosmol. Astropart. Phys. 6 (2009) 035.

[44] M. Kawasaki, T. Takahashi, and S. Yokoyama, Density fluctuations in thermal inflation and non-Gaussianity, J. Cosmol. Astropart. Phys. 12 (2009) 012.

[45] J. Elliston, D. J. Mulryne, D. Seery, and R. Tavakol, Evolution of fNL to the adiabatic limit, J. Cosmol. Astropart. Phys. 11 (2011) 005.

[46] G. Leung, E. R. M. Tarrant, C. T. Byrnes, and E. J Copeland, Reheating, multifield inflation and the fate of the primordial observables, J. Cosmol. Astropart. Phys. 9 (2012) 008.

[47] J. Elliston, S. Orani, and D. J. Mulryne, General analytic predictions of two-field inflation and perturbative reheating, Phys. Rev. D **89**, 103532 (2014).

[48] C. T. Byrnes, K.-Y. Choi, and L. M. H. Hall, Large non-Gaussianity from two-component hybrid inflation, J. Cosmol. Astropart. Phys. 2 (2009) 017.

[49] A. Naruko and M. Sasaki, Large Non-Gaussianity from multi-brid inflation, Prog. Theor. Phys. **121**, 193 (2009).

[50] S. A. Kim and A. R. Liddle, Nflation: Non-Gaussianity in the horizon-crossing approximation, Phys. Rev. D **74**, 063522 (2006).

[51] S. A. Kim, A. R. Liddle, and D. Seery, Non-Gaussianity in Axion N-flation Models, Phys. Rev. Lett. **105**, 181302 (2010).

[52] D. Langlois and L. Sorbo, Primordial perturbations and non-Gaussianities from modulated trapping, J. Cosmol. Astropart. Phys. 8 (2009) 014.

[53] K. Nakayama and T. Suyama, Curvature perturbation from velocity modulation, Phys. Rev. D **84**, 063520 (2011).

[54] C. M. Peterson and M. Tegmark, Non-Gaussianity in two-field inflation, Phys. Rev. D **84**, 023520 (2011).

[55] C. M. Peterson and M. Tegmark, Testing multi-field inflation: A geometric approach, Phys. Rev. D **87**, 103507 (2013).

[56] L. Alabidi, K. Malik, C. T. Byrnes, and K.-Y. Choi, How the curvaton scenario, modulated reheating and an inhomogeneous end of inflation are related, J. Cosmol. Astropart. Phys. 11 (2010) 037.

[57] C. T. Byrnes, M. Cortês, and A. R. Liddle, Comprehensive analysis of the simplest curvaton model, Phys. Rev. D **90**, 023523 (2014).

[58] R. J. Hardwick and C. T. Byrnes, Bayesian evidence of the post-Planck curvaton, J. Cosmol. Astropart. Phys. 8 (2015) 010.

[59] T. L. Smith and D. Grin, Probing a panoply of curvaton-decay scenarios using CMB data, Phys. Rev. D **94**, 103517 (2016).

[60] V. Vennin, K. Koyama, and D. Wands, Encyclopædia curvatonis, J. Cosmol. Astropart. Phys. 11 (2015) 008.

[61] V. Vennin, K. Koyama, and D. Wands, Inflation with an extra light scalar field after Planck, J. Cosmol. Astropart. Phys. 3 (2016) 024.

[62] A. A. Starobinskiǐ, Multicomponent de Sitter (inflationary) stages and the generation of perturbations, Sov. J. Exp. Theor. Phys. Lett. **42**, 152 (1985).

[63] M. Sasaki and E. D. Stewart, A General analytic formula for the spectral index of the density perturbations produced during inflation, Prog. Theor. Phys. **95,** 71 (1996).

[64] D. H. Lyth and Y. Rodríguez, Inflationary Prediction for Primordial Non-Gaussianity, Phys. Rev. Lett. **95,** 121302 (2005).

[65] F. Vernizzi and D. Wands, Non-Gaussianities in two-field inflation, J. Cosmol. Astropart. Phys. 5 (2006) 019.

[66] T. Kobayashi, F. Takahashi, T. Takahashi, and M. Yamaguchi, Spectator field models in light of spectral index after Planck, J. Cosmol. Astropart. Phys. 10 (2013) 042.

[67] K. Enqvist and T. Takahashi, Mixed inflaton and spectator field models after Planck, J. Cosmol. Astropart. Phys. 10 (2013) 034.

[68] L. Wang, Spectator fields and their imprints on the Cosmic Microwave Background, arXiv:1610.03123.

[69] T. Suyama, T. Takahashi, M. Yamaguchi, and S. Yokoyama, Implications of Planck results for models with local type non-Gaussianity, J. Cosmol. Astropart. Phys. 6 (2013) 012.

[70] S. Renaux-Petel, Primordial non-Gaussianities after Planck 2015: An introductory review, C.R. Phys. **16,** 969 (2015).

[71] J. M. Bardeen, P. J. Steinhardt, and M. S. Turner, Spontaneous creation of almost scale-free density perturbations in an inflationary universe, Phys. Rev. D **28,** 679 (1983).

[72] D. Wands, K. A. Malik, D. H. Lyth, and A. R. Liddle, A New approach to the evolution of cosmological perturbations on large scales, Phys. Rev. D **62,** 043527 (2000).

[73] S. Weinberg, Adiabatic modes in cosmology, Phys. Rev. D **67,** 123504 (2003).

[74] S. Weinberg, Must cosmological perturbations remain non-adiabatic after multi-field inflation?, Phys. Rev. D **70,** 083522 (2004).

[75] S. Weinberg, Non-Gaussian correlations outside the horizon II: The general case, Phys. Rev. D **79,** 043504 (2009).

[76] J. Meyers, Non-Gaussian correlations outside the horizon in local thermal equilibrium, arXiv:1212.4438.

[77] D. Wands, Local non-Gaussianity from inflation, Classical Quantum Gravity **27,** 124002 (2010).

[78] M. Sasaki, J. Valiviita, and D. Wands, Non-Gaussianity of the primordial perturbation in the curvaton model, Phys. Rev. D **74,** 103003 (2006).

[79] G. Leung, E. R. M. Tarrant, C. T. Byrnes, and E. J. Copeland, Reheating, multifield inflation and the fate of the primordial observables, J. Cosmol. Astropart. Phys. 09 (2012) 008.

[80] J. Meyers and E. R. M. Tarrant, Perturbative Reheating After Multiple-Field Inflation: The Impact on Primordial Observables, Phys. Rev. D **89,** 063535 (2014).

[81] M. A. Amin, M. P. Hertzberg, D. I. Kaiser, and J. Karouby, Nonperturbative dynamics of reheating after inflation: A review, Int. J. Mod. Phys. D **24,** 1530003 (2015).

[82] D. Seery and J. E. Lidsey, Primordial non-Gaussianities from multiple-field inflation, J. Cosmol. Astropart. Phys. 9 (2005) 011.

[83] D. Wands, N. Bartolo, S. Matarrese, and A. Riotto, Observational test of two-field inflation, Phys. Rev. D **66,** 043520 (2002).

[84] E. Nelson and S. Shandera, Statistical naturalness and non-Gaussianity in a finite universe, Phys. Rev. Lett. **110,** 131301 (2013).

[85] S. Nurmi, C. T. Byrnes, and G. Tasinato, A non-Gaussian landscape, J. Cosmol. Astropart. Phys. 6 (2013) 004.

[86] M. LoVerde, E. Nelson, and S. Shandera, Non-Gaussian mode coupling and the statistical cosmological principle, J. Cosmol. Astropart. Phys. 6 (2013) 024.

[87] L. Alabidi and D. H. Lyth, Inflation models and observation, J. Cosmol. Astropart. Phys. 5 (2006) 016.

[88] N. Kobayashi, T. Kobayashi, and A. L. Erickcek, Rolling in the modulated reheating scenario, J. Cosmol. Astropart. Phys. 1 (2014) 036.

[89] J. Meyers and E. R. M. Tarrant, Perturbative reheating after multiple-field inflation: The impact on primordial observables, Phys. Rev. D **89,** 063535 (2014).

[90] A. Linde, Particle Physics and Inflationary Cosmology, ArXiv High Energy Physics—Theory e-prints (Mar., 2005), arXiv:hep-th/0503203.

[91] K. Ichikawa, T. Suyama, T. Takahashi, and M. Yamaguchi, Primordial curvature fluctuation and its non-Gaussianity in models with modulated reheating, Phys. Rev. D **78,** 063545 (2008).

[92] K. Kamada, K. Kohri, and S. Yokoyama, Affleck-Dine baryogenesis with modulated reheating, J. Cosmol. Astropart. Phys. 1 (2011) 027.

[93] Planck Collaboration, P. A. R. Ade et al., Planck 2015 results. XX. Constraints on inflation, Astron. Astrophys. **594,** A20 (2016).

[94] P. A. R. Ade et al. (BICEP2, Planck Collaboration), Joint Analysis of BICEP2/Keck?Array and Planck Data, Phys. Rev. Lett. **114,** 101301 (2015).

[95] D. Foreman-Mackey, D. W. Hogg, D. Lang, and J. Goodman, Emcee: The MCMC Hammer, Publ. Astron. Soc. Pac. **125,** 306 (2013).

[96] Planck Collaboration, P. A. R. Ade et al., Planck 2015 results. XIII. Cosmological parameters, Astron. Astrophys. **594,** A13 (2016).

[97] D. H. Lyth and A. Riotto, Particle physics models of inflation and the cosmological density perturbation, Phys. Rep. **314,** 1 (1999).

[98] T. Banks, M. Dine, P. J. Fox, and E. Gorbatov, On the possibility of large axion decay constants, J. Cosmol. Astropart. Phys. 06 (2003) 001.

[99] P. Svrcek and E. Witten, Axions in string theory, J. High Energy Phys. 06 (2006) 051.